The *C9ORF72* repeat expansion alters neurodevelopment

Eric Hendricks[1,2,3], **Alicia M. Quihuis**[3,4], **Shu-Ting Hung**[1,2,3], **Jonathan Chang**[1,2,3], **Nomongo Dorjsuren**[1,2,3], **Balint Der**[1,2], **Kim A. Staats**[1,2], **Yingxiao Shi**[1,2,3], **Naomi S. Sta Maria**[3,4], **Russell E. Jacobs**[3,4], **Justin K. Ichida**[1,2,3,5,*]

[1]Department of Stem Cell Biology and Regenerative Medicine, Keck School of Medicine, University of Southern California, Los Angeles, CA 90033, USA

[2]Eli and Edythe Broad CIRM Center for Regenerative Medicine and Stem Cell Research, University of Southern California, Los Angeles, CA 90033, USA

[3]Zilkha Neurogenetic Institute, Keck School of Medicine, University of Southern California, Los Angeles, CA 90033, USA

[4]Department of Physiology and Neuroscience, Keck School of Medicine, University of Southern California, Los Angeles, CA 90033, USA

[5]Lead contact

SUMMARY

Genetic mutations that cause adult-onset neurodegenerative diseases are often expressed during embryonic stages, but it is unclear whether they alter neurodevelopment and how this might influence disease onset. Here, we show that the most common cause of frontotemporal dementia (FTD) and amyotrophic lateral sclerosis (ALS), a repeat expansion in *C9ORF72*, restricts neural stem cell proliferation and reduces cortical and thalamic size *in utero*. Surprisingly, a repeat expansion-derived dipeptide repeat protein (DPR) not known to reduce neuronal viability plays a key role in impairing neurodevelopment. Pharmacologically mimicking the effects of the repeat expansion on neurodevelopment increases susceptibility of *C9ORF72* mice to motor defects. Thus, the C9ORF72 repeat expansion stunts development of the brain regions prominently affected in *C9ORF72* FTD/ALS patients.

In brief

The C9ORF72 repeat expansion alters neural stem cell maintenance, leading to reduced thalamic volume and cortical thickness in prenatal mice. This effect is mediated by interaction of the dipeptide repeat protein poly(AP) with the ribosomal maturation factor LRRC47. Impairing neurodevelopment accelerates onset of motor deficits in C9ORF72 mice.

*Correspondence: ichida@usc.edu.

Graphical Abstract
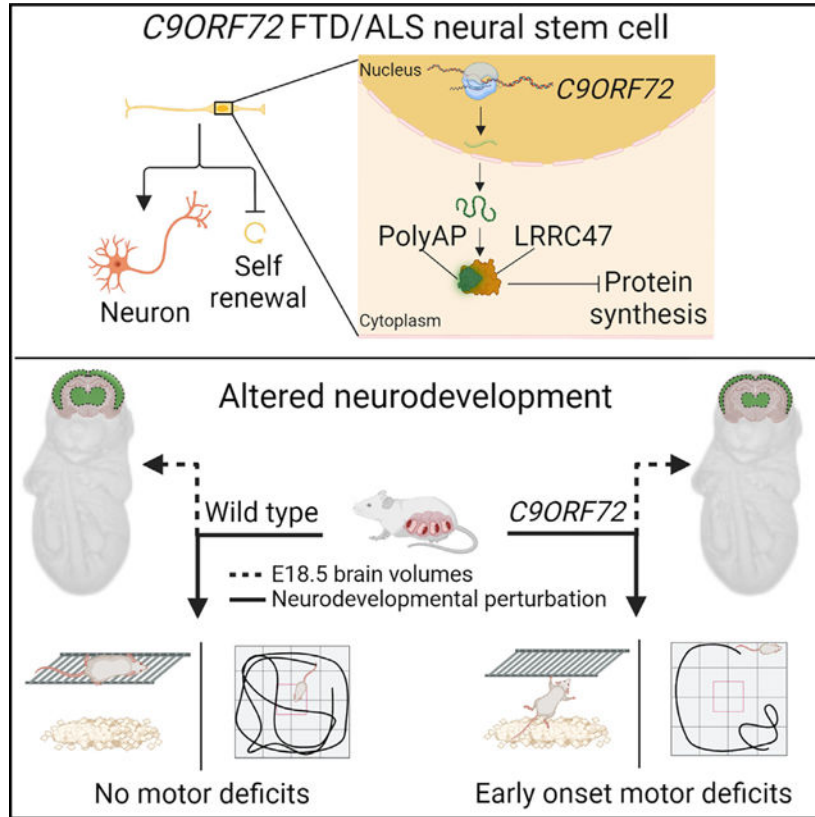
INTRODUCTION

Many genes containing mutations that cause adult-onset neurodegenerative disease are expressed early in life, but it remains unclear whether the mutations alter the neurodevelopmental trajectory and, therefore, potentially impact disease onset in adulthood.[1,2] Recent studies show that the Huntington's disease-causing CAG repeat expansion in *Huntingtin* leads to reduced neonatal brain volume in mice and humans.[3,4] Moreover, reducing Huntingtin levels only during development in mice still leads to neurodegeneration in adulthood, even when normal Huntingtin levels are restored after post-natal day 21.[3] These findings argue that expression of neurodegenerative disease-causing gene mutations during embryonic or neonatal periods can alter neurodevelopment in ways that increase susceptibility to neurodegenerative disease. However, it is unclear whether other neurodegenerative disease-causing mutations, including other repeat expansions, alter neurodevelopment.

An intronic hexanucleotide GGGGCC repeat expansion in *C9ORF72* is the most common known cause of amyotrophic lateral sclerosis (ALS) and frontotemporal dementia (FTD) and accounts for 5%–10% of each disease.[5,6] Analyses of induced pluripotent stem cell (iPSC) mouse models and patient tissue indicate that the repeat expansion reduces C9ORF72

protein levels and leads to repeat-associated non-AUG translation of dipeptide repeat proteins (DPRs) and accumulation of repeat expansion-containing RNA foci.[5–10]

Intriguingly, imaging studies indicate that *C9ORF72* repeat expansion carriers display reduced gray and white matter volumes in thalamic and frontal cortical regions as early as the fourth decade of life, 10–20 years before the average age of disease onset.[11,12] Presymptomatic *C9ORF72* repeat expansion carriers also display prominent connectivity deficits in salience and medial pulvinar thalamus-seeded networks, suggesting that the structural changes havefunctionalconsequences.[11–13] Importantly, the gray matter deficits in presymptomatic repeat expansion carriers are topographically similar to atrophied brain regions in *C9ORF72* FTD patients, suggesting that the presymptomatic structural changes have meaningful consequences for *C9ORF72* patients.

A key question is whether the presymptomatic gray matter reductions in *C9ORF72* repeat expansion carriers arise from altered development or early degeneration. If the structural changes arise from altered development, then the magnitude of these changes in a given carrier may help to predict disease onset and progression years in advance. On the other hand, if the gray matter reductions reflect presymptomatic neurodegeneration, then it would greatly elevate the importance of initiating therapeutic treatment much earlier, even before symptom onset when possible. Several lines of evidence suggest that the structural changes might reflect altered neurodevelopment. First, gray and white matter volumes decline with age at a similar rate in *C9ORF72* repeat expansion carriers and non-carriers, suggesting degeneration within the 10- to 20-year period preceding disease onset does not cause structural differences between the two groups.[12] Second, while cerebrospinal fluid (CSF) levels of the neurodegeneration biomarker neurofilament light chain increase in repeat expansion carriers after symptom onset, they remain low before disease onset, suggesting that there is limited neurodegeneration presymptomatically.[12,14] Third, *C9ORF72* is expressed in the nervous system during embryonic and neonatal periods in mice and humans, indicating that the repeat expansion could affect neurodevelopment.[15–18] However, it remains unclear whether the *C9ORF72* repeat expansion alters neurodevelopment, how it might elicit such effects, and how structural changes acquired during development would affect symptom onset.

Here, we show that the *C9ORF72* repeat expansion restricts neural stem cell proliferation and reduces thalamic and cortical size *in utero*. Mechanistically, we find that loss of C9ORF72 function does not appreciably alter neural stem and progenitor cell behavior. Instead, unexpectedly, the non-neurotoxic DPR poly(alanine-proline) (poly(AP)) plays a key role in reducing the number of neural stem and progenitor cells in *C9ORF72* ALS/FTD iPSC cultures. Poly(AP) induces this effect in part by binding to a ribosomal maturation factor called LRRC47 and lowering protein synthesis.[19] We find that a peptide that impairs neurodevelopment increases the frequency of motor defects in *C9ORF72*-bacterial artificial chromosome (BAC) mice. Thus, our findings suggest that the *C9ORF72* repeat expansion impairs the development of brain regions prominently affected in *C9ORF72* FTD/ALS patients, which could potentially affect the emergence of disease symptoms later in life.

RESULTS

C9ORF72 FTD/ALS neural stem cells exhibit poor self-renewal and precocious differentiation

To determine whether the *C9ORF72* repeat expansion alters neurodevelopment, we derived neural stem and progenitor cells from 4 control and 4 *C9ORF72* FTD/ALS patient iPSC lines that we had used previously to identify neuronal changes induced by the repeat expansion (Table S1).[9,20] To control for differences in genetic background, we used a previously generated CRISPR-Cas9-derived isogenic control from our lab, or "corrected" line, by removing the *C9ORF72* repeat expansion from one patient line (Table S1).[21] Repeat-primed PCR analysis confirmed the presence of the *C9ORF72* repeat expansion in *C9ORF72* FTD/ALS lines and its absence in controls, and we previously verified removal of the repeat expansion in the corrected line by Southern blot (Figure S1B; Table S2).[21] To generate cortical neural stem and progenitor cells from iPSCs, we used a previously published protocol that employed retinoid treatment and dual SMAD inhibition (Figure 1A).[22] On day 10 of differentiation, we performed magnetic activated cell sorting (MACS) purification of polysialic acid-neural cell adhesion molecule (PSA-NCAM)+ cells to enrich for neural precursors (Figure 1A).[23] Immunocytochemical analysis showed that almost 100% of cells were positive for the neural stem cell markers PAX6 and NESTIN after MACS purification (Figures S1C and S1D). As expected, bulk RNA sequencing (RNA-seq) analysis showed that the control, *C9ORF72* FTD/ALS, and corrected PSA-NCAM+ cells expressed high levels of cortical stem cell markers, including *PAX6*, *OTX1*, *OTX2*, and *SOX2*, and low levels of ventral and caudal neural stem cell markers and pluripotent stem cell markers (Figure S1E; Tables S3 and S4; 4 control and 4 *C9ORF72* FTD/ALS donors, 1 corrected line).

To determine the ability of day 10 MACS-purified neural stem and progenitor cells to self-renew, we further cultured them in epidermal growth factor (EGF) and fibroblast growth factor (FGF) to promote maintenance of the neural stem cell and progenitor states. After an additional 5 or 20 days under these conditions (days 15 and 30 total), we used immunocytochemistry to quantify the percentage of neural stem/progenitor cells or neurons by quantifying the fraction of cells that were PAX6+ or MAP2+, respectively, among all DAPI+ cells (Figure 1A). On day 15, *C9ORF72* FTD/ALS cultures showed striking reductions in the percentages of PAX6+ and Ki67+ dividing cells compared with the control and corrected lines (Figures 1B–1D; 4 control and 4 *C9ORF72* FTD/ALS donors, 1 corrected line). In addition, while the PAX6+ cells in control and corrected cultures displayed structures with apicobasal polarity reminiscent of the cortical ventricular zone, *C9ORF72* FTD/ALS cultures exhibited fewer of these rosette-like structures (Figures 1E–1G; 4 control and 4 *C9ORF72* FTD/ALS donors, 1 corrected line). Cleaved caspase-3 immunocytochemistry indicated that these differences did not result from increased cell death in *C9ORF72* FTD/ALS cultures (Figures S1F and S1G). In contrast to the reductions in neural stem and progenitor cells on day 15, *C9ORF72* FTD/ALS cultures possessed more neurons than control and corrected cultures on day 30 (Figures 1H–1J; 4 control and 4 *C9ORF72* FTD/ALS donors, 1 corrected line). Consistent with these phenotypic differences, bulk RNA-seq analysis of day 10 PSA-NCAM+ MACS-sorted neural cultures

from 4 control and 4 *C9ORF72* FTD/ALS lines showed differential expression of genes involved in nervous system development and neuron differentiation and generation (Figure S1H). Thus, under culture conditions intended to promote neural stem cell maintenance, *C9ORF72* FTD/ALS neural stem and progenitor cells exhibited reduced self-renewal and rosette formation while undergoing increased differentiation into neurons.

Poly(AP) and other *C9ORF72* DPRs impair neural stem cell self-renewal

We have shown previously that reduced C9ORF72 function because of the repeat expansion contributes to neurodegeneration in iPSC-derived motor neurons.[9,23] Because *C9ORF72* was highly expressed in day 10 MACS-purified PSA-NCAM+ cells (in the top 15% of all expressed genes), we determined whether loss of C9ORF72 function accounted for the impaired self-renewal of *C9ORF72* FTD/ALS neural stem and progenitor cells (Table S3). We differentiated neural cultures from a control line and an isogenic *C9ORF72*$^{-/-}$ line we had generated previously by using CRISPR-Cas9 editing to introduce frameshift mutations into both copies of *C9ORF72* (Figure S2A and S2B).[9] Western blot analysis confirmed that these mutations eliminated full-length C9ORF72 protein in day 10 MACS-purified PSA-NCAM+ cells derived from the *C9ORF72*$^{-/-}$ isogenic line (Figures S2C and S2D). After culturing day 10 MACS-purified PSA-NCAM+ cells for 5 additional days in EGF and FGF, there were no significant differences in the percentages of PAX6+ or Ki67+ cells between control and *C9ORF72*$^{-/-}$ cultures (Figures 2A and 2B).

In addition to reducing C9ORF72 protein function, the repeat expansion induces gain-of-function processes, including production of 5 different DPR species through repeat-associated, non-AUG translation of the sense and antisense *C9ORF72* transcripts.[9,10,24] We found previously that, among the 5 DPRs, poly(GR) and poly(PR) cause severe neurotoxicity when overexpressed individually, whereas poly(AP), poly(glycine-alanine [GA]), and poly(glycine-proline [GP]) did not significantly affect neuronal survival.[10] Immunocytochemistry using knockout or previously validated antibodies showed that day 10 PAX6+ neural stem and progenitor cells from *C9ORF72* FTD/ALS patients possessed DPRs derived from the sense and antisense *C9ORF72* transcripts, including poly(AP), poly(GR), and poly(PR) (Figures 2C–2E and S2E–S2J).[20,25–28] In contrast, PAX6+ neural stem and progenitor cells from the corrected line and non-isogenic controls did not (Figures 2C–2E and S2E–S2J; 4 control and 3 *C9ORF72* FTD/ALS donors, 1 corrected line). While poly(GR) and poly(PR) showed punctate staining patterns, poly(AP) appeared more diffuse in neural stem and progenitor cells (Figures 2C–2E and S2E–S2J). These DPR staining patterns were consistent with results from a previously published cell culture study.[25]

To determine whether DPRs impair neural stem cell self-renewal, we overexpressed 50-repeat versions of each DPR in day 10 MACS-purified PSA-NCAM+ cells derived from control lines. These 50-repeat DPR constructs were equivalent to the ones we and others tested previously in neurons.[9,10] After 5 days of additional culture with EGF and FGF, we quantified the percentage of PAX6+ and Ki67+ cells under each DPR condition in 4 different control lines. Similar to their mild effects on neuronal survival in a previous study, poly(GA) and poly(GP) did not affect the percentage of PAX6+ neural stem and progenitor cells or Ki67+ dividing cells (Figures 2F–2H; 4 control donors).[10]

In contrast, the neurotoxic poly(GR) and poly(PR) DPRs significantly reduced the percentage of Ki67+ dividing cells while leading to a slight reduction in the percentage of PAX6+ cells (Figures 2F–2H; 4 control donors). Surprisingly, while poly(AP) has been shown previously to be non-toxic to neurons, it significantly reduced the percentage of PAX6+ cells and slightly lowered the fraction of Ki67+ dividing cells (Figures 2F–2H; 4 control donors).[10] Using antisense oligonucleotide (ASO) treatment to reduce levels of the antisense *C9ORF72* transcript, which gives rise to poly(AP) and poly(PR), significantly increased the number of PAX6+ neural stem and progenitor cells in *C9ORF72* FTD/ALS cultures (Figures S2K–S2N).

Poly(AP) impairs neural stem cell maintenance through LRRC47

Because poly(AP) most severely reduced the percentage of PAX6+ neural stem and progenitor cells over 5 days of culture in EGF and FGF, and this marker was most directly linked to neural progenitor cells, we investigated the mechanisms through which poly(AP) mediated this effect. To identify interactors of poly(AP), we overexpressed 50-repeat poly(AP) (AP(50)-GFP) or GFP alone in day 10 MACS-purified PSA-NCAM+ cells from 2 different control lines, immunoprecipitated AP(50)-GFP or GFP on day 15 using an anti-GFP antibody, and analyzed the co-immunoprecipitated proteins by mass spectrometry. This experiment identified 3 proteins that co-immunoprecipitated with AP(50)-GFP to a greater extent than GFP alone (Table S5). These proteins included glucose-6-phosphate isomerase (GPI), aldehyde dehydrogenase 16 family member A1 (ALDH16A1), and leucine-rich repeat-containing 47 (LRRC47) (Table S5). Of these top candidate proteins, co-immunoprecipitation experiments in which GFP or AP(50)-GFP was immunoprecipitated using a GFP-specific antibody verified that endogenous LRRC47 interacted with AP(50)-GFP significantly more than PR(50)-GFP or GFP alone (Figures 3A and 3B).

A recent cryo-electron microscopy study showed that LRRC47 participates in ribosomal maturation in human cells and binds to pre-40S ribosomes in the late stages of small ribosomal subunit formation.[10,19] To determine whether poly(AP) interferes with the ability of LRRC47 to interact with the pre-40S ribosome, we measured the amount of the 40S subunit ribosomal protein S6 (RPS6) that co-immunoprecipitated with an LRRC47-FLAG-mCherry fusion protein in the presence or absence of poly(AP). While RPS6 clearly co-immunoprecipitated with the LRRC47-FLAG-mCherry fusion protein when immunoprecipitated from GFP-overexpressing cells with a FLAG-specific antibody, it did not co-immunoprecipitate with FLAG-mCherry alone, indicating that it interacted with LRRC47 but not FLAG-mCherry (Figures 3C and 3D). Importantly, compared with GFP overexpression, AP(50)-GFP significantly reduced the amount of endogenous RPS6 that co-immunoprecipitated with LRRC47-FLAG-mCherry, suggesting that poly(AP) interfered with the ability of LRRC47 to interact with the pre-40S ribosome (Figures 3C and 3D). We determined whether this impacted protein synthesis in day 15 PSA-NCAM MACS-purified neural stem and progenitor cells by using L-homopropargylglycine (HPG), a methionine analog that contains an alkene moiety that enables covalent linkage to a dye after incorporation into proteins during translation.[29] Indeed, AP(50)-GFP expression significantly reduced HPG incorporation in control PAX6+ neural stem and progenitor cells

compared with GFP alone, suggesting that poly(AP) lowered protein synthesis (Figures 3E and 3F; 4 control donors).

We next asked whether LRRC47 activity modulates neural stem cell self-renewal by reducing *LRRC47* expression using ASOs. Indeed, ASO-mediated suppression of *LRRC47* in day 10 MACS-purified PSA-NCAM+ cells from control individuals significantly reduced the percentage of PAX6+ cells after 5 days of culture with EGF and FGF (Figures 3G–3I; 4 control donors). Conversely, we determined whether increasing *LRRC47* expression could mitigate the loss of neural stem and progenitor cells in *C9ORF72* FTD/ALS lines or control lines overexpressing AP(50)-GFP. Transducing day 10 PSA-NCAM+ cells with a *LRRC47*-mCherry lentivirus increased PAX6+ neural stem and progenitor cells in *C9ORF72* FTD/ALS lines and control lines overexpressing AP(50)-GFP compared with mCherry alone (Figures 3J–3M; 3 *C9ORF72* FTD/ALS donors and 4 control donors + AP(50)-GFP). Our results suggest that poly(AP) reduces the number of PAX6+ cells and lowers protein synthesis through its interaction with LRRC47. Poly(GR) and poly(PR) bind to ribosomes and can also impair protein synthesis, and these effects may also affect neural progenitor function.[30]

The *C9ORF72* repeat expansion reduces thalamic and cortical size in embryonic mice

C9ORF72 repeat expansion carriers display reduced thalamic and cortical volumes many years or even decades before the average age of disease onset.[11–13] This raises the possibility that the *C9ORF72* repeat expansion causes developmental changes affecting brain structure *in vivo*. Because our *in vitro* experiments indicated that patient-derived neural stem and progenitor cells display limited self-renewal capacity, we next asked whether the *C9ORF72* repeat expansion similarly impairs neurodevelopment *in vivo*. First, we performed a meta-analysis derived from multiple studies to evaluate the expression of *Lrrc47* at various stages of development. The analysis revealed detectable *Lrrc47* expression via single-cell RNA-seq as early as embryonic day 9.5 (E9.5) in neural progenitor cells and across 9 brain regions in adult mice (Figures S3A and S3C).[31,32] Thus, DPRs in the developing mouse embryo brain might interact with Lrrc47, similar to what we observed in our *in vitro* data (Figures 3A–3D). To investigate the presence of DPRs derived from the C9ORF72 repeat expansion during early development, we examined transgenic mice harboring a BAC containing a patient-derived *C9ORF72* repeat expansion.[33,34] Although the extent of neurodegenerative phenotypes in these mice has varied in different colonies, multiple studies have confirmed the presence of DPRs and the repeat expansion, the two key drivers of impaired neural stem cell self-renewal in our study.[33–35] To assess the presence of DPRs in developing *C9ORF72*-BAC embryos, we performed immunohistochemical analysis on tissue from E9.5–E11.5 mice using knockout or previously validated DPR antibodies.[20,25–28] Because human imaging studies indicated that cortical and thalamic regions showed some of the largest reductions in brain volume in presymptomatic *C9ORF72* repeat expansion carriers, we examined DPR levels in the cortex and thalamus and used PAX6 and OLIG2 to identify cortical and thalamic neural progenitor cells, respectively.[36,37] This analysis, coupled with a strand-specific linker qRT-PCR strategy to quantify the amount of antisense transcripts derived from the *C9ORF72*-BAC construct, confirmed the presence of poly(AP)+, poly(GR)+, and poly(PR)+ puncta in cortical and thalamic

progenitor cells in *C9ORF72*-BAC embryos but not controls (Figures 4A–4F and S3D–S3J). Consistent with the notion that the *C9ORF72* repeat expansion impairs neural progenitor proliferation, *C9ORF72*-BAC embryos possessed fewer PAX6+/Ki67+ cells in the developing telencephalon at E9.5 (Figures 4G and 4H) Similar to our *in vitro* findings and published work, while poly(AP) formed some puncta, its staining pattern was more diffuse than poly(GR) and poly(PR) (Figures 2C, S2E, S2H, S3D, S3F, and S3H).[25]

We next examined E18.5 embryos to investigate any developmental differences induced by the *C9ORF72* repeat expansion. E18.5 *C9ORF72*-BAC embryos weighed about 5%–10% less than non-transgenic controls, suggesting that the repeat expansion impacted development beyond the nervous system (Figure S3K). This is consistent with the multi-tissue expression pattern of *C9ORF72* (proteinatlas.org). Magnetic resonance imaging showed that, when normalized to body weight, there was no difference in total brain volume between *C9ORF72*-BAC and control embryos (Figures 4I and 4J). However, we observed a 50% reduction in thalamic volume relative to total brain volume in *C9ORF72*-BAC embryos (Figures 4I and 4K). Immunohistochemical analysis of the thalamus confirmed these findings and showed a similar 50% decrease in thalamic size in *C9ORF72*-BAC embryos (Figures 4L and 4M). In addition, assessment of the mid-rostral neocortex by immunohistochemistry and magnetic resonance imaging indicated that cortical thickness relative to total brain area was reduced by about 20% in *C9ORF72*-BAC embryos (Figures 4N, 4O, S3L, and S3M). These data indicated that the *C9ORF72* repeat expansion altered brain structure in developing mouse embryos.

Vasoactive intestinal peptide (VIP) antagonism enhances symptom onset in *C9ORF72*-BAC mice

We next wondered whether impaired neurodevelopment might reduce the ability of the nervous system to cope with neurodegenerative processes caused by *C9ORF72* repeat expansion. To investigate the effect of altered neurodevelopment on the emergence of ALS/FTD-like manifestations in *C9ORF72*-BAC, we used a VIP antagonist during gestation to impair neurodevelopment in control and *C9ORF72*-BAC mice. During pregnancy, VIP is secreted from maternal lymphocytes, crosses the placental barrier, and exerts a major growth effect on the central nervous system.[38] Intraperitoneal injection of pregnant mice with a peptide VIP antagonist containing only the receptor-binding portion of VIP but not the signaling component can block VIP signaling in developing embryos.[39,40] VIP antagonist treatment during neurogenesis from E9.5–E11.5 disrupts neuroepithelial progenitor proliferation and promotes cell cycle exit and precocious neuronal differentiation.[40] In the resulting progeny, this treatment reduces cortical thickness by about 20%–40% while preserving cortical structure and cell type composition.[40] In contrast to their reduced cortical thickness, VIP antagonist-treated neonates have normal body weight.[40] Therefore, VIP antagonist treatment from E9.5–E11.5 provides a potential tool for modifying the neurodevelopmental trajectory and determining how this affects the timing of *C9ORF72* symptom onset *in vivo*.

To examine the effect of impairing neurodevelopment on disease phenotypes in *C9ORF72*-BAC mice, we treated pregnant dams with vehicle or VIP antagonist from E9.5–E11.5.

Consistent with published results, mice exposed to the VIP antagonist displayed an ~10% reduction in brain mass (Figures 5A and 5B).[40] Immunohistochemical analysis confirmed that VIP antagonist treatment reduced cortical thickness by 30%–40% in control and *C9ORF72*-BAC embryos at E18.5 (Figures 5C and 5D). Because *C9ORF72*-BAC embryos already possessed thinner cortices because of the repeat expansion, *in utero* VIP antagonist treatment of these embryos resulted in severely reduced cortical thickness (Figures 5C and 5D). Although this reduction was beyond that caused by the repeat expansion alone, it nevertheless allowed us to determine how the severity of neurodevelopmental impairment affects symptom onset. To assess this, we measured motor function by hanging wire and open field tests at 2 months of age. No published studies have observed motor dysfunction in *C9ORF72*-BAC mice at this young age.[33–35] Consistent with these studies, vehicle-treated 2 month-old *C9ORF72*-BAC mice showed no motor dysfunction compared with vehicle-treated controls (Figures 5E and 5F). In contrast, VIP antagonist-treated *C9ORF72*-BAC mice displayed a markedly shorter latency to fall in the hanging wire test and a significantly shorter distance traveled in a timed open field test compared with vehicle-treated *C9ORF72*-BAC mice (Figures 5E and 5F). VIP antagonist-treated control mice showed no differences from vehicle-treated controls in these experiments (Figures 5E and 5F). Although we cannot rule out the possibility that VIP antagonism during development leads to permanent gene expression changes in adulthood that can themselves alter hanging wire and open field test performance, our results suggest that impaired neurodevelopment may enhance disease symptoms in *C9ORF72*-BAC mice.

DISCUSSION

We find that the *C9ORF72* repeat expansion impairs neurodevelopment in mice and human stem cell cultures. Embryonic *C9ORF72*-BAC mice displayed large reductions in thalamic size and cortical thickness, which bears striking resemblance to published observations in presymptomatic human *C9ORF72* repeat expansion carriers.[11–14] The magnitudes of thalamic and cortical size reductions we observed in embryonic *C9ORF72*-BAC mice are consistent with the possibility that neurodevelopmental changes could explain why *C9ORF72* repeat expansion carriers display reduced thalamic and cortical volumes decades before disease onset.

Surprisingly, our data indicate that poly(AP), a DPR not known to affect neurodegeneration, plays a key role in restricting neural stem and progenitor cell self-renewal. Our investigation revealed an interaction between poly(AP) and ribosomal maturation factor LRRC47. Poly(AP) significantly reduced the ability of LRRC47 to interact with the 40S ribosome protein RPS6 and lowered total protein synthesis rates in neural stem and progenitor cell cultures. Reducing LRRC47 in control neural stem and progenitor cells impaired self-renewal, and overexpressing LRRC47 increased self-renewal when poly(AP) was ectopically expressed and in *C9ORF72* FTD/ALS neural stem and progenitor cells. Although additional studies will be needed to confirm these findings *in vivo*, these results suggest that poly(AP)'s effect on LRRC47 function greatly impacts neural stem cell self-renewal. Poly(PR) and poly(GR) may also impact neural stem cell function, although they preferentially reduced the number of Ki67+ cells rather than PAX6+ cells in our cultures.

This may be because they impair protein synthesis to a different degree or with a different bias than poly(AP) or because they affect other cellular functions.[30]

Our VIP antagonist experiments in mice suggest that increasing the extent of neurodevelopmental impairment sensitizes mice to the emergence of disease symptoms caused by the *C9ORF72* repeat expansion. This may have significant implications for our understanding of disease onset in *C9ORF72* repeat expansion carriers. The penetrance of the *C9ORF72* repeat expansion is incomplete, and age of disease onset varies widely, ranging from 40–90 years of age.[41] The reasons for the incomplete penetrance and varied disease onset are unclear, but the reductions in brain volume in presymptomatic *C9ORF72* repeat expansion carriers are also heterogeneous.[11–14] It will require further investigation to determine whether the timing of disease onset in C9ORF72 repeat expansion carriers is determined by the extent of neurodevelopmental alterations, genetic modifiers, or environmental effects. Understanding these factors could greatly improve our ability to predict disease onset and treat *C9ORF72* carriers at early stages of disease.

Limitations of the study

Regarding the use of VIP antagonism to disrupt neurodevelopment and evaluate its impact on *C9ORF72*-induced behavioral phenotypes in mice, we cannot rule out the possibility that VIP antagonism led to permanent gene expression changes in adulthood that altered hanging wire and open field test performance independent of C9ORF72 pathogenesis rather than enhancing the pathogenic effects of the *C9ORF72* repeat expansion. In future studies, we hope to employ a genetic conditional approach to activate *C9ORF72* pathology at different time points in mice pre- and postnatally to better determine how embryonic expression of the *C9ORF72* repeat expansion might contribute to C9ORF72 disease later in life. Also, future studies should determine whether the extent of early structural changes in the brains of *C9ORF72* carriers correlates with the time of disease onset. Another limitation is that, because of technical limitations, we did not provide *in vivo* confirmation that loss of LRRC47 because of the repeat expansion is responsible for impaired neurodevelopment. It will be important to verify this in future studies. We will also explore the effects of poly(PR) and poly(GR) on neurodevelopment. Further studies utilizing these approaches will be essential in guiding our interpretation of the role of neurodevelopmental deficits in the onset and progression of neurodegeneration during adulthood.

STAR★METHODS

RESOURCE AVAILABILITY

Lead contact—Further information and requests for resources and reagents should be directed to and will be fulfilled by the lead contact, Justin Ichida (ichida@usc.edu).

Materials availability—Human iPSC lines generated in this study are available upon request from the lead contact.

Data code and availability—RNA sequencing data have been deposited at NCBI's Gene Expression Omnibus (GEO) and are accessible through GEO Series accession number

GSE238005. The RNA sequencing data are publicly available as of the date of publication. The accession number is also listed in the key resources table. This paper does not report original code. Any additional information required to reanalyze the data reported in this paper is available from the lead contact upon request.

EXPERIMENTAL MODEL AND STUDY PARTICIPANT DETAILS

Cell lines—Human iPSC lines were derived by the Ichida lab using lymphoblastoid lines obtained from the NINDS Biorepository (Table S1). Both male and female iPSC lines were included in the study. These iPSCs were maintained in mTeSR1 medium following a feeder-free culture protocol and cultured in six-well plates coated with growth Geltrex. The iPSC cultures were incubated at 37°C with 5% CO2, and they were fed daily with 2mL of mTeSR medium per well. To maintain consistency, the cultures were kept below 90% confluency. Whenever required, iPSC colonies were passaged using Accutase (Innovative Cell Technologies) at the desired split ratio.

Mouse model—Wild-type FVB/NJ (strain: 001800) and FVB/NJ-Tg(C9orf72)500Lpwr/J (strain: 029099) were purchased from Jackson Laboratories (The Jackson Laboratory, Bar Harbor, USA). Mice were housed in standard conditions with food and water ad *libitum* in the conventional vivarium at the University of Southern California. Both male and female mice were used in this study. All animal use and care were in accordance with local institution guidelines of the University of Southern California and the IACUC board of the University of Southern California (Los Angeles, USA) under protocol number 11938.

METHOD DETAILS

CRISPR/Cas9 genome editing of iPSCs—CRISPR/Cas9-mediated genome editing was performed in human iPSCs as previously described by Ran et al., 2013. To generate isogenic control iPSCs by removing the repeat expansion, single guide RNAs (sgRNAs) targeting both sides of the *C9ORF72* intronic hexanucleotide repeat expansion were designed (Table S2, http://crispr.mit.edu) and cloned into an empty gRNA cloning vector (Addgene ID: 31824). The donor plasmid for homologous recombination was generated by PCR-amplifying left and right homology arms (588 bp and 1149 bp, respectively) from control genomic DNA into the pUC19 vector with an added puro^r cassette. 2×10^6 *C9ORF72* ALS/FTD line 1 iPSCs were transfected with human codon-optimized Cas9 (Addgene ID: 31825), the appropriate gRNA constructs by nucleofection (Lonza) according to the manufacturer's protocol, and the homologous recombination donor vector. The cells were replated on wells precoated with Geltrex (Life Technologies) in mTeSR1 medium supplemented with 10 μm Y-27632 (Selleck). Y-27632 was removed on the next day followed by puromycin selection (7.5 μg/ml) for 48 h. On day 7 after transfection, the surviving colonies were manually picked and genotyped by sequencing the targeted genomic site. Colonies showing removal of the repeat expansion were clonally purified by plating 1000 iPSCs on a 10-cm dish of irradiated MEF feeders in human ESC medium (DMEM/F12, 20% knockout serum replacement, 1% non-essential amino acids, 1% Glutamax, 1X penicillin/streptomycin (all Life Technologies), 0.1% beta mercaptoethanol (Sigma), and 10 ng/mL bFGF (Peprotech)) and re-picking of the resulting colonies. Normalization of *C9ORF72* was verified by southern blotting.

***C9ORF72* southern blotting**—A 241-bp digoxigenin (DIG)-labeled probe was generated from 100 ng control genomic DNA (gDNA) by PCR reaction using Q5 High-Fidelity DNA Polymerase (NEB) with primers shown in Table S2. Genomic DNA was harvested from control and patient iPSCs using cell lysis buffer (100 mM Tris-HCl pH 8.0, 50 mM EDTA, 1% w/v sodium dodecyl sulfate (SDS)) at 55°C overnight and performing phenol:chloroform extraction. A total of 25 μg of gDNA was digested with AflII at 37°C overnight, run on a 0.8% agarose gel, then transferred to a positive charged nylon membrane (Roche) using suction by vacuum and UV-crosslinked at 120 mJ. The membrane was pre-hybridized in 25 mL DIG EasyHyb solution (Roche) for 3 h at 47°C then hybridized at 47°C overnight in a shaking incubator, followed by two 5-min washes each in 2X Standard Sodium Citrate (SSC) and in 0.1% SDS at room temperature, and two 15-min washes in 0.1x SSC and in 0.1% SDS at 68°C. Detection of the hybridized probe DNA was carried out as described in DIG System User's Guide. CDP-Star Chemilumnescent Substrate (Sigma-Aldrich) was used for detection and the signal was developed on X-ray film (Genesee Scientific) after 20 to 40 min.

Repeat primed PCR (RP-PCR)—To provide a quantitative measure of the $(GGGGCC)_n$ hexanuceotide expansion in *C9ORF72*, 20 ng/μL of genomic DNA was isolated with a DNeasy blood & tissue kit (Qiagen, cat. no. 69504) and amplified by PCR in a 20-μL PCR reaction consisting of 1 μM primer 1 (FAM-tgtaaaacgacggccagtCAAGGAGGGAAACAACCGCAGCC), 1 μM primer 2 (caggaaacagctatgaccGGGCCCGCCCCGAC CACGCCCCGGCCCCGGCCCCGG), 1 μM primer 3 (caggaaacagctatgacc), 1x Qiagen buffer (Qiagen, cat. no. 201203), 2.5 units Taq polymerase (Qiagen, cat. no. 201203), 0.25 mM dCTP, 0.25 mM dATP, 0.25 mM dTTP, 0.25 mM 7-deaza-2-deoxy GTP (NEB, cat. no. N0445S), 5% DMSO, 1 M betaine (Sigma, cat. no. B0300–1VL). The PCR protocol was as follows: [98°C 10 min], 1 cycle; [97°C 35 s, 64°C 2 min, 68°C 8 min], 10 cycles; [97°C 35 s, 64°C 2 min, 68°C 8–16 min], 25 cycles with an additional 20 s added to the extension step each cycle. The PCR products were directly analyzed using an ABI3730 DNA Analyzer and Peak Scanner Software v1.0 (Life Technologies).

Conversion of iPSCs to neural stem and progenitor cells—iPSCs were initially seeded in mTesr1 with the addition of rock inhibitor (Selleckchem, cat. no. S1049) on 6-well plates (7×10^5 cells/well) that were coated with geltrex (1:100 dilution) for 1 h at 37°C (day 0). Directed differentiation began when the cells reached 85% confluency by performing a half media change with a knockout serum replacement media containing DMEM/F12 (Thermo Fisher Scientific, cat. no. 11320033), 15% KOSR (Thermo Fisher Scientific, cat. no. 10828028), 1x NEAA (Thermo, cat. no. 11140050), 1x glutamax (Thermo, cat. no. 35050061), 10 μM SB 431542 (Cayman chemical, cat. no. 13031), and 100 nM LDN-193189 (Cayman chemical, cat. no. 11802). A full media change with the knockout serum replacement media described above was performed on day 3 and day 4. On day 5 and day 6, the media was switched to an N2 media containing DMEM/F12, 1x NEAA, 1x glutamax, 1x N2 supplement (Thermo Fisher, cat no. 17502–048), 10 μM SB 431542, and 100 nM LDN-193189. A media change using N2 media without the dual SMAD inhibitors (SB 431542 and LDN-193189) was performed on days 7–9. Cells were passaged with

accutase (Thermo, cat. no. A1110501) and PSA-NCAM MACS purified on day 10 or 15 and were maintained with daily media changes containing DMEM/F12, 1x B27 supplement (Thermo Fisher, cat no. 17504044), 1x N2 supplement, 1x NEAA, 1x Glutamax, 10 ng/mL EGF (R&D Systems, cat. no. 236-EG-200), and 10 ng/mL FGF (R&D Systems, cat. no. 3718-FB-025).

Magnetic-activated cell sorting of PSA-NCAM+ neural stem and progenitor cells—Day 10 neural stem cell cultures were passaged with accutase and centrifuged for 5 min at 1000 rpm in DMEM. The supernatant was removed, and the cell pellets were resuspended (100 μL per 10×10^6 cells) in staining media containing 1% BSA in PBS and incubated on ice for 10 min. After this initial incubation, 20 μL of anti-PSA-NCAM magnetic microbeads (Miltenyi, cat. no. 130–092-966) were added to the suspension and incubated on ice for 15 min. The suspension was washed with 3 mL of staining media and centrifuged at 1000 rpm for 5 min. The supernatant was removed, and the cell pellet was resuspended in 500 μL of staining media. LS columns (Miltenyi, cat. no. 130–042-401) were placed on a MACS multi-stand (Miltenyi, cat. no. 130–042-303) and equilibrated with 3 mL of staining media. After equilibration, the 500 μL cell suspension was added to the column and washed 3 times with 3 mL of staining media by gravity filtration. Next, the LS column was removed from the MACS multi-stand, 7 mL of staining media was added to the column, and the PSA-NCAM+ cells were plunged into a clean 15 mL conical tube. The suspension was centrifuged at 1000 rpm for 5 min and resuspended in neural stem cell maintenance media containing rock inhibitor.

Immunocytochemistry—Cells were fixed in 4% paraformaldehyde (PFA) for 30 min at room temperature, permeabilized with 0.5% PBS-triton x-100 for 15 min at room temperature, blocked with 10% FBS in 0.1% PBS-T at room temperature for 1 h, and incubated with primary antibodies at 4°C overnight. Cells were then washed with 0.1% PBS-T and incubated with Alexa Fluor secondary antibodies (Life Technologies, 1:500) in blocking buffer for 1 h at room temperature. To visualize nuclei, cells were stained with DAPI (Invitrogen, 1:1000) then mounted on slides with Vectashield (Vector Labs). Images were acquired on an LSM 800 confocal microscope (Zeiss). The following primary antibodies were used: mouse anti-PAX6 (Thermo Fisher Scientific, cat. No. MA1–109, 1:500), rabbit anti-KI67 (GeneTex, cat no. GTX16667, 1:500), chicken anti-MAP2 (Abcam, cat. No. ab5392, 1:1000), rabbit anti-caspase-3 (Abcam, cat. no. ab13847, 1:500) rabbit anti-PolyAP (Proteintech, cat. no. 24493–1-AP, 1:500), rabbit anti-PolyPR (Proteintech, cat. no. 23979–1-AP, 1:500), rabbit anti-PolyGR (Proteintech, cat. no. 23978–1-AP, 1:500).

Quantification of PAX6 and KI67 immunocytochemistry—iPSC-derived neural stem cells underwent magnetic-activated cell sorting of PSA-NCAM+ to enrich for neural stem and progenitor cells at Day 10 of differentiation. The enriched population was plated at a density of 3×10^4 per well in 96-well plates. The cells were maintained in the media described above and exposed to 10 ng/mL of both EGF and FGF for 5 days with media changes occurring every other day. A batch processing script in ImageJ (https://imagej.net/scripting/batch) was used to automate the detection of DAPI, PAX6, and KI67 after fixation and staining (previously described) to determine percentages of PAX6+ or KI67+ cells out

of total DAPI+ cells. The brightness and contrast were optimized using a control line and then utilized to process all samples. The script code is available upon request.

Rosette quantification—iPSC-derived neural stem cells underwent magnetic-activated cell sorting of PSA-NCAM+ to enrich for neural stem and progenitor cells at Day 10 of differentiation. The enriched population was plated at a density of 3×10^4 per well in 96-well plates. The cells were maintained in the media described above and exposed to 10 ng/mL of both EGF and FGF for 5 days with media changes occurring every other day. Cells were fixed after 5 days (Day 15) and stained for PAX6. Cultures displayed multicellular structures of neuroepithelial tissue with an apicobasal polarity reminiscent of the cortical ventricular zone. These structures were manually counted for each well for each cell line.

Quantification of MAP2+ cells—iPSC-derived neural stem cells underwent magnetic-activated cell sorting of PSA-NCAM+ to enrich for neural stem and progenitor cells at Day 10 of differentiation. The enriched population were plated onto coverslips at a density of 5×10^5 per well in 24-well plates. The cells were maintained in the media described above and exposed to 10 ng/mL of both EGF and FGF for 20 days with media changes occurring every other day. The coverslips were fixed and stained for MAP2 as described above. Images were taken with an LSM 780 confocal microscope. MAP2+ cell somas were counted and quantified as a fraction of the total number of DAPI+ cells to determine the percentage of MAP2+ cells in the field of view.

Production of lentiviruses—HEK293T cells were transfected at 80–90% confluency with viral vectors containing mCherry (Genecopoeia, cat. no. EX-NEG-Lv216), LRRC47-mCherry (Genecopoeia, cat. no. EX-T4416-Lv216), GFP, GA(50)-GFP, GP(50)-GFP, PR(50)-GFP, GR(50)-GFP AP(50)-GFP (GFP-containing constructs were gifted from the Trotti Laboratory); and viral packaging plasmids pPAX2 and VSVG using polyethylenimine (PEI)(Sigma-Aldrich). The medium was changed 24 h after transfection. Viruses were harvested at 48 h and 72 h after transfection. Viral supernatants were filtered with 0.45 μM filters, incubated with Lenti-X concentrator (Clontech) for 24 h at 4°C, and centrifuged at 1,500 x g at 4C for 45 min. The pellets were resuspended in 100 μL of DMEM and stored at −80°C.

Bulk RNA sequencing—Day 10 PSA-NCAM+ MACS-purified cells (5×10^5) were lysed in RLT buffer (Qiagen, cat. no. 79216) and sent to Amaryllis Nucleics for library preparation and sequencing. All FASTQ files were analyzed by Ji Informatics using FastQC (version 0.11.5) and aligned using the HISAT2 (v2–2.1.0). The resulting transcripts were tested for differential expression using DEseq2 (version 1.18.1). Pathway enrichment analysis was performed using Enrichr.

AP(50)-GFP and GFP co-immunoprecipitation with endogenous LRRC47— HEK293T cells were transfected with GFP and AP(50)-GFP lentiviral constructs in 10 cm dishes according to our transfection protocol described above. Cells were lysed in 500 μl of ice-cold Pierce IP lysis buffer (ThermoFisher, cat. no. 87787) containing 1x protease inhibitor cocktail (Sigma, cat. no. 4693132001) 5 days post-transfection. Lysates were incubated on ice for 1 h with periodic mixing by inversion and subsequently centrifuged at

14,000 g for 15 min at 4°C. The resulting supernatants were transferred to new Eppendorf tubes and the co-IP was performed following the manufacturers protocol for the SDS elution using the GFP-trap magnetic particles M-270 kit (Chromotek, cat. no. gtdk-20). Briefly, 200 μL of cell lysate was diluted with 300 μL of the provided dilution buffer and 25 μL of equilibrated GFP-trap magnetic beads was added. The solution was incubated overnight at 4°C with end-over-end rotation. Next, the beads were washed three times with the provided wash buffer, resuspended in 80 μL of 2x SDS-sample buffer, boiled for 5 min at 95°C, and analyzed via Western Blot using anti-GFP (Aves, cat. no. GFP-1010, 1:1000) and rabbit anti-LRRC47 (Proteintech, cat. no. 23217–1-AP, 1:500). LRRC47 protein detected was endogenous LRRC47. Images were acquired using an LI-COR Odyssey CLx.

Co-immunoprecipitation of LRRC47-FLAG-mCherry and endogenous RPS6—
HEK293T cells plated in 10 cm dishes were transfected with lentiviral DNA constructs encoding an LRRC47-FLAG-mCherry fusion protein and GFP, LRRC47-FLAG-mCherry and AP(50)-GFP, or FLAG-mCherry alone, and an untransfected sample group was also included. Cells were lysed in 500 μl of ice-cold Pierce IP lysis buffer (ThermoFisher, cat. no. 87787) containing 1x protease inhibitor cocktail (Sigma, cat. no. 4693132001) 5 days post-transfection. Lysates were incubated on ice for 1 h with periodic mixing by inversion and subsequently centrifuged at 14,000 g for 15 min at 4°C. The resulting supernatants were transferred to new Eppendorf tubes. Since the LRRC47 lentiviral construct contains an FLAG tag, anti-FLAG M2 magnetic beads (Sigma, cat. no. M8823) were used to immunoprecipitate LRRC47-FLAG-mCherry or FLAG-mCherry to determine its interaction with RPS6. First, 20 μL of beads were equilibrated by washing twice with 200 μL of 1x TBS on a magnetic stand. The entire sample lysate was added to the beads and incubated overnight at 4°C with end-over-end rotation. After this incubation, the beads were washed 3x with 500 μL of 1x TBS. The samples were eluted with 50 μL of 3x FLAG peptide (150 ng/μL)(Sigma, cat. no. F4799). The samples were placed on a magnetic stand after a 30 min incubation at room temperature with the 3x FLAG peptide and the supernatants were transferred to clean Eppendorf tubes. Western blots were performed with an anti-LRRC47 antibody (Proteintech, cat. no. 23217–1-AP, 1:500) to detect LRRC47-FLAG-mCherry and an anti-RPS6 antibody (Thermofisher, cat. no. MA5–15123, 1:500) to detect endogenous RPS6.

Homopropargylglycine protein synthesis assay—Neural stem and progenitor cells overexpressing AP(50)-GFP or GFP alone were assayed for protein synthesis 5 days post-infection using the manufacturers protocol for the Click-iT HPG Alexa Fluor 594 protein synthesis assay kit (ThermoFisher, cat. no. C10429). In short, the cells were cultured with L-homopropargylglycine (HPG) in neural stem cell media devoid of L-methionine for 30 min at 37°C on coverslips. Cells were fixed with 4% paraformaldehyde for 15 min at room temperature. Cells were washed twice with 3% BSA in PBS and permeabilized with 0.5% Triton X-100 in PBS for 20 min at room temperature. HPG signal was detected using Click-IT chemistry detected via Alexa Fluor 594 azide. Images were acquired using a Zeiss LSM800 confocal microscope.

Quantitative real-time PCR—Total RNA was extracted from MACs purified PSA-NCAM+ neural stem and progenitor cells at day 15 with an RNeasy plus mini kit (Qiagen, cat. no. 74136) and reverse transcribed with an Oligo dT primer using ProtoScript II First Strand Synthesis Kit (NEB, cat. no. 102855–124). RNA concentration and purity was checked using the NanoDrop One (ThermoFisher). Real-time PCR was performed with iTaq Universal SYBR Green Supermix (Bio-Rad) using primers shown in Table S2.

ASO—Antisense oligonucleotides (ASOs) were synthesized by Integrated DNA Technologies. A concentration of 9 μM was administered with treatment lasting 5 days for all ASO experiments. Knockdown efficiency was determined by qRT-PCR. ASO sequences are shown in Table S2.

Mass spectrometry—A total of three 10 cm dishes of MACs purified PSA-NCAM+ neural stem and progenitor cells from two healthy controls overexpressing AP(50)-GFP or GFP alone were lysed in 500 ml of ice-cold Pierce IP lysis buffer (ThermoFisher, cat. no. 87787) containing 1x protease inhibitor cocktail (Sigma, cat. no. 4693132001) 5 days post-infection for each condition. Lysates were incubated on ice for 1 h with periodic mixing by inversion and subsequently centrifuged at 14,000 g for 15 min at 4°C. The resulting supernatants were transferred to new Eppendorf tubes and GFP was pulled down using GFP-trap magnetic particles M-270 kit (Chromotek, cat. no. gtdk-20). The entire 500 μL cell lysate for each condition was used for the pulldown by adding 50 μL of equilibrated GFP-trap magnetic beads to the lysates. The solution was incubated overnight at 4C with end-over-end rotation. Next, the beads were washed three times with the provided wash buffer, resuspended in 80 μL of 2x SDS-sample buffer, boiled for 5 min at 95°C, and an in-gel digestion was performed with trypsin. Standard desalting and peptide enrichment was performed and the samples were run on a Thermo Easy nLC Q-Exactive at the Beckman Institute Proteome Exploration Lab at Caltech (Pasadena, CA).

Western blot—MACs-sorted PSA-NCAM+ neural stem and progenitor cells from healthy controls and C9-FTD/ALS patients were collected in RIPA buffer (Sigma-Aldrich) with a protease inhibitor cocktail (Roche). Protein quantity was measured by the BCA assay (Pierce) and samples were run on a 10% SDS gel at room temperature in with compatible loading buffers for the LI-COR Odyssey CLx. The gel was transferred onto a nitrocellulose membrane (VWR) via a semi-dry transfer. The membrane was blocked with intercept blocking buffer (Licor, cat. no. 927–60010) for 1 h at room temperature, incubated with primary antibodies overnight at 4°C, washed three times with 0.1% PBS-T, then incubated with the appropriate IRDye (Licor, 1:5000) for 1 h at room temperature. After five washes with PBS, blots were visualized using an LI-COR Odyssey CLx. Sample signals were normalized based on the revert 700 total protein stain (Licor). The following primary antibodies were used: rabbit anti-LRRC47 (Proteintech, cat. no. 23217–1-AP, 1:500), chicken anti-GFP (Aves, cat. no. GFP-1010, 1:1000), rabbit anti-C9ORF72 (Proteintech, cat. no. 22637–1-AP, 1:500), and ribosomal protein S6 (Thermofisher, cat. no. MA5–15123, 1:500).

Animal care and breeding—Wild-type FVB/NJ (strain: 001800) and FVB/NJ-Tg(C9orf72)500Lpwr/J (strain: 029099) were purchased from Jackson Laboratories (The Jackson Laboratory, Bar Harbor, USA). Mice were housed in standard conditions with food and water ad *libitum* in the conventional vivarium at the University of Southern California. Heterozygous male mice harboring the repeat expansion were used to breed with wild-type female mice. Mice were genotyped using the following PCR protocol: [94°C 3 min], 1 cycle; [94°C 45 s, 55°C 45 s, 72°C 1 min], 32 cycles; [72°C 6 min], 1 cycle (primers listed in Table S2). All animal use and care were in accordance with local institution guidelines of the University of Southern California and the IACUC board of the University of Southern California (Los Angeles, USA) under protocol number 11938.

E9.5 mouse embryo immunohistochemistry and quantification—Control pregnant dams crossed with male *C9ORF72*-BAC were identified based on vaginal plugs (E0.5). The dams were euthanized 9 days after plug identification and the embryos were extracted and fixed for 1 h in 4% PFA at 4°C. Cryoprotection occurred in 30% sucrose. After snap freezing, the tissue was sectioned by cryostat at 14 μm thickness, permeabilized with 0.5% Triton X- in PBS, and subjected to antigen retrieval. The antigen retrieval solution (10 mM sodium citrate at pH 6.0) was preheated for 1 min in the microwave and then added to the coupling jars with the sectioned tissue. The tissue incubated in the antigen retrieval solution for 30 min in a vegetable steamer, subsequently blocked with 10% FBS in PBS for 1 h, and stained with the following primary antibodies overnight at 4°C in 10% FBS/0.1% PBST: mouse anti-PAX6 (Santa Cruz Biotechnology, cat. no. sc-81649, 1:100), rabbit anti-PAX6 (Biolegend, cat. no. 901301, 1:100), chicken anti-NESTIN (Novus Biologicals, cat. no. NB100–1604, 1:500), mouse anti-KI67 (BD Biosciences, cat. no. 550609, 1:100), goat anti-OLIG2 (R&D Systems, cat. no. AF2418, 1:100), rabbit anti-Poly(AP) (Proteintech, cat. no. 244931-AP, 1:100), rabbit anti-Poly(GR) (Proteintech, cat. no. 23978–1-AP, 1:100), and rabbit anti-Poly(PR) (Proteintech, cat. no. 239791-AP, 1:100). Images were collected using a Zeiss LSM800 confocal microscope. Nuclear puncta of poly(AP), poly(GR), and poly(PR) were quantified in PAX6 and OLIG2 positive cells in ImageJ.

Strand specific quantitative real-time PCR—We followed the protocol as previously described by Zu et al.[43] Total RNA was extracted from whole brain tissue in E18.5 embryos via a RNeasy plus mini kit. The cDNA was generated from 0.25 μg of total RNA using the ProtoScript II First Strand Synthesis Kit with LK strand-specific reverse primers (LK-AS-ORF-R) and PCR with strand-specific forward (AS-ORF-F) and LK primer shown in Table S2. Real-time PCR was performed with iTaq Universal SYBR Green Supermix (Bio-Rad).

Quantification of PAX6 and KI67 double-positive cells—E9.5 mouse embryos were sectioned and stained for PAX6 and KI67 as described above. The spot colocalization plugin (ComDet v.0.5.0) in ImageJ was used to quantify the number of PAX6 and KI67 double-positive cells in the telencephalon in E9.5 mouse embryos. The following were baseline parameters for the colocalization plugin and modified to determine the best fit for each image: max distance between particles = 8, Ch1a pixels = 4, Ch1a intensity = 5, Ch2i pixels = 7, and Ch2i intensity = 9.

VIP antagonist administration—Pregnant dams were identified by the presence of vaginal plugs, which was used to calculate the timing of vasoactive intestinal peptide (VIP) receptor antagonist injections. Pregnant dams were administered intraperitoneal (IP) injections of 2 μg/g body weight of the VIP receptor antagonist compound (Tocris, cat. no. 3054) once a day at E9.5, E10.5, and E11.5. The effect of VIP receptor antagonism on brain size was assessed at E18.5 and 2 months of age.

Magnetic resonance imaging of E18.5 embryos—E18.5 embryos were imaged using a 7 Tesla PET-MR system (MR Solutions Ltd., Guildford, UK) housed at the Zilkha Neurogenetic Institute Functional Biological Imaging Core, with a bore size of ~24 cm, up to 600 mT/m maximum gradient, and a 20 mm internal diameter quadrature birdcage coil. To increase our signal to noise ratio we incubated the embryos in ProHance (10:1 v/v saline/Pro-hance) overnight prior to imaging. A three dimensional (3D) T2-weighted Fast Spin Echo (FSE) sequence was used with the following parameters: repetition time (TR) = 300 ms, echo time (TE) = 48 ms, field of view (FOV) = 18 mm × 18 mm x 18 mm, matrix size = $256 \times 256 \times 256$, isotropic voxel size = 70.3125 μm, number of averages (NA) = 18, echo train length = 17, and flip angle (FA) = 90. Total acquisition time was approximately 14 h. We used VivoQuant software to manually quantify the thalamus from coronal slices derived from the 3D scan and an embryo atlas was used as a guide to verify thalamic specificity (https://sectional-anatomy.org/mouse-embryo/). Approximately 12 sections of the total brain scanned overlapped with the thalamus. Total brain volumes were acquired in a similar manner for each embryo to normalize thalamic volume (thalamic volume/total brain volume). The normalized values were then calculated to represent the relative changes in volume compared to control embryos. 3D rendering of the images was performed in Imaris.

E18.5 mouse embryo immunohistochemistry and quantification of thalamic area and cortical thickness—Control pregnant dams crossed with male *C9ORF72*-BAC were identified based on vaginal plugs (E0.5). The dams were euthanized 18 days after plug identification and the embryos were extracted and fixed overnight in 4% PFA at 4°C. Cryoprotection occurred in 30% sucrose. After snap freezing, the tissue was sectioned by cryostat at 16 μm thickness and stained with DAPI (Invitrogen, 1:1000) and Neurotrace (Thermo Fisher Scientific, cat. no. N21480, 1:100) for 20 min at room temperature. Tissue sections were washed 5 times with PBS and mounted using Vectashield. Images were taken using a Zeiss Axiozoom microscope. Thalamic area was outlined in ImageJ from 4 sections per embryo beginning at approximately bregma +3.51 and 3 subsequent sections 16 μm apart. These values were averaged for each embryo in both genotypes and the values were represented as the ratio relative to WT. Cortical thickness was measured by extending a vertical line in ImageJ from layer1 to layer 6 in 10 different regions along the mid-rostral neocortex in 3 different sections per embryo. These values were averaged and represented as either relative ratios (Figure 4) or raw values (Figure 5).

Open field test and hanging wire assay—At 2 months of age, VIP antagonist receptor treated and PBS treated mice for both control and *C9ORF72*-BAC were placed in the designated behavioral room for 30 min prior to the open field test in order to acclimate to the testing room environment. After acclimation, mice were placed in a 44 cm × 44 cm x 30.5

cm clear plastic box and total distance was tracked over 15 min via the Noldus Ethovision software. The open field boxes were cleaned before and after each trial with 70% ethanol.

Motor function was also assessed for each treatment group via hanging wire. To begin, the mice were placed on a cage top elevated approximately 20 cm above the cage floor. The top was inverted and the latency to fall was recorded. Test performance was averaged for 3 separate trials for each mouse.

Cortical thickness quantification of MRI images—MRI images were converted from DICOM to NIFTI format using an open source software described in Li et al.(Li et al., 2016). Orientations of the converted MRI images were adjusted to be in the transverse orientation using a reorientation software described by Heuer et al. 2020 for E18.5 control (n = 8) and *C9ORF72*-BAC (n = 15) embryos. Cortical thickness was averaged using ImageJ across ten subsections with 6 measurements for each subsection between the pineal gland and 4th ventricle. The cortical thickness measurements were normalized to the average total brain area across the ten subsections for each embryo. The scientist performing the cortical thickness quantification was blinded to the genotypes of the samples.

QUANTIFICATION AND STATISTICAL ANALYSIS

For all datasets, we determined normality using GraphPad Prism and applied the appropriate single or multiple comparison test. For all graphs, each data point consists of a biological replicate, which is defined specifically in each figure legend.

Supplementary Material

Refer to Web version on PubMed Central for supplementary material.

ACKNOWLEDGMENTS

DECLARATION OF INTERESTS

J.K.I. is a co-founder of AcuraStem, Inc. and Modulo Bio. J.K.I. is on the scientific advisory board of AcuraStem, Inc.; Spinogenix; and Vesalius Therapeutics. J.K.I. is an employee of BioMarin Pharmaceutical. J.K.I. is a co-founder of Modulo Bio and serves on the scientific advisory board of Spinogenix. Named companies were not involved in this project.

INCLUSION AND DIVERSITY

We support inclusive, diverse, and equitable conduct of research. One or more of the authors of this paper self-identifies as an underrepresented ethnic minority in their field of research or within their geographical location. One or more of the authors of this paper self-identifies as a gender minority in their field of research. One or more of the authors of this paper self-identifies as a member of the LGBTQIA+ community. One or more of the authors of this paper received support from a program designed to increase minority representation in their field of research.

REFERENCES

1. Deneubourg C, Ramm M, Smith LJ, Baron O, Singh K, Byrne SC,Duchen MR, Gautel M, Eskelinen E-L, Fanto M, and Jungbluth H. (2022). The spectrum of neurodevelopmental, neuromuscular and neurodegenerative disorders due to defective autophagy. Autophagy 18, 496–517. 10.1080/15548627.2021.1943177. [PubMed: 34130600]

2. Schor NF, and Bianchi DW (2021). Neurodevelopmental Clues to Neurodegeneration. Pediatr. Neurol. 123, 67–76. 10.1016/j.pediatrneurol.2021.07.012. [PubMed: 34399111]

3. Arteaga-Bracho EE, Gulinello M, Winchester ML, Pichamoorthy N, Petronglo JR, Zambrano AD, Inocencio J, De Jesus CD, Louie JO, Gokhan S, et al. (2016). Postnatal and adult consequences of loss of huntingtin during development: Implications for Huntington's disease. Neurobiol. Dis. 96, 144–155. 10.1016/j.nbd.2016.09.006. [PubMed: 27623015]

4. Barnat M, Capizzi M, Aparicio E, Boluda S, Wennagel D, Kacher R,Kassem R, Lenoir S, Agasse F, Braz BY, et al. (2020). Huntington's disease alters human neurodevelopment. Science 369, 787–793. 10.1126/science.aax3338. [PubMed: 32675289]

5. DeJesus-Hernandez M, Mackenzie IR, Boeve BF, Boxer AL, Baker M, Rutherford NJ, Nicholson AM, Finch NA, Flynn H, Adamson J, et al. (2011). Expanded GGGGCC hexanucleotide repeat in noncoding region of C9ORF72 causes chromosome 9p-linked FTD and ALS. Neuron 72, 245–256. 10.1016/j.neuron.2011.09.011. [PubMed: 21944778]

6. Renton AE, Majounie E, Waite A, Simón-Sánchez J, Rollinson S, Gibbs JR, Schymick JC, Laaksovirta H, van Swieten JC, Myllykan-gas L, et al. (2011). A Hexanucleotide Repeat Expansion in C9ORF72 Is the Cause of Chromosome 9p21-Linked ALS-FTD. Neuron 72, 257–268. 10.1016/j.neuron.2011.09.010. [PubMed: 21944779]

7. Donnelly CJ, Zhang P-W, Pham JT, Haeusler AR, Mistry NA, Vi-densky S, Daley EL, Poth EM, Hoover B, Fines DM, et al. (2013). RNA toxicity from the ALS/FTD C9ORF72 expansion is mitigated by antisense intervention. Neuron 80, 415–428. 10.1016/j.neuron.2013.10.015. [PubMed: 24139042]

8. Lagier-Tourenne C, Baughn M, Rigo F, Sun S, Liu P, Li H-R, Jiang J, Watt AT, Chun S, Katz M, et al. (2013). Targeted degradation of sense and antisense C9orf72 RNA foci as therapy for ALS and frontotemporal degeneration. Proc. Natl. Acad. Sci. USA 110, E4530–E4539. 10.1073/pnas.1318835110. [PubMed: 24170860]

9. Shi Y, Lin S, Staats KA, Li Y, Chang W-H, Hung S-T, Hendricks E, Linares GR, Wang Y, Son EY, et al. (2018). Haploinsufficiency leads to neurodegeneration in C9ORF72 ALS/FTD human induced motor neurons. Nat. Med. 24, 313–325. 10.1038/nm.4490. [PubMed: 29400714]

10. Wen X, Tan W, Westergard T, Krishnamurthy K, Markandaiah SS, Shi Y, Lin S, Shneider NA, Monaghan J, Pandey UB, et al. (2014). Antisense proline-arginine RAN dipeptides linked to C9ORF72-ALS/FTD form toxic nuclear aggregates that initiate in vitro and in vivo neuronal death. Neuron 84, 1213–1225. 10.1016/j.neuron.2014.12.010. [PubMed: 25521377]

11. Bertrand A, Wen J, Rinaldi D, Houot M, Sayah S, Camuzat A, Fournier C, Fontanella S, Routier A, Couratier P, et al. (2018). Early Cognitive, Structural, and Microstructural Changes in Presymptomatic C9orf72 Carriers Younger Than 40 Years. JAMA Neurol. 75, 236–245. 10.1001/jamaneurol.2017.4266. [PubMed: 29197216]

12. Lee SE, Sias AC, Mandelli ML, Brown JA, Brown AB, Khazenzon AM, Vidovszky AA, Zanto TP, Karydas AM, Pribadi M, et al. (2017). Network degeneration and dysfunction in presymptomatic C9ORF72 expansion carriers. Neuroimage. Clin. 14, 286–297. 10.1016/j.nicl.2016.12.006. [PubMed: 28337409]

13. De Vocht J, Blommaert J, Devrome M, Radwan A, Van Weehaeghe D, De Schaepdryver M, Ceccarini J, Rezaei A, Schramm G, van Aalst J, et al. (2020). Use of Multimodal Imaging and

Clinical Biomarkers in Presymptomatic Carriers of C9orf72 Repeat Expansion. JAMA Neurol. 77, 1008–1017. 10.1001/jamaneurol.2020.1087. [PubMed: 32421156]

14. Meeter LHH, Gendron TF, Sias AC, Jiskoot LC, Russo SP, Donker Kaat L, Papma JM, Panman JL, van der Ende EL, Dopper EG, et al. (2018). Poly(GP), neurofilament and grey matter deficits in expansion carriers. Ann. Clin. Transl. Neurol. 5, 583–597. 10.1002/acn3.559. [PubMed: 29761121]

15. Atkinson RAK, Fernandez-Martos CM, Atkin JD, Vickers JC, and King AE (2015). C9ORF72 expression and cellular localization over mouse development. Acta Neuropathol. Commun. 3, 59. 10.1186/s40478-015-0238-7. [PubMed: 26408000]

16. Bennett ML, Bennett FC, Liddelow SA, Ajami B, Zamanian JL, Fernhoff NB, Mulinyawe SB, Bohlen CJ, Adil A, Tucker A, et al. (2016). New tools for studying microglia in the mouse and human CNS. Proc. Natl. Acad. Sci. USA 113, E1738–E1746. 10.1073/pnas.1525528113. [PubMed: 26884166]

17. Zhang Y, Chen K, Sloan SA, Bennett ML, Scholze AR, O'Keeffe S, Phatnani HP, Guarnieri P, Caneda C, Ruderisch N, et al. (2014). An RNA-Sequencing Transcriptome and Splicing Database of Glia, Neurons, and Vascular Cells of the Cerebral Cortex. J. Neurosci. 34, 11929–11947. 10.1523/jneurosci.1860-14.2014. [PubMed: 25186741]

18. Zhang Y, Sloan SA, Clarke LE, Caneda C, Plaza CA, Blumenthal PD, Vogel H, Steinberg GK, Edwards MSB, Li G, et al. (2016). Purification and Characterization of Progenitor and Mature Human Astrocytes Reveals Transcriptional and Functional Differences with Mouse. Neuron 89, 37–53. 10.1016/j.neuron.2015.11.013. [PubMed: 26687838]

19. Ameismeier M, Zemp I, van den Heuvel J, Thoms M, Berninghausen O, Kutay U, and Beckmann R. (2020). Structural basis for the final steps of human 40S ribosome maturation. Nature 587, 683–687. 10.1038/s41586-020-2929-x. [PubMed: 33208940]

20. Shi Y, Hung S-T, Rocha G, Lin S, Linares GR, Staats KA, Seah C, Wang Y, Chickering M, Lai J, et al. (2019). Identification and therapeutic rescue of autophagosome and glutamate receptor defects in C9ORF72 and sporadic ALS neurons. JCI Insight 5, e127736. 10.1172/jci.insight.127736.

21. Hung S-T, Linares GR, Chang W-H, Eoh Y, Krishnan G, Mendonca S, Hong S, Shi Y, Santana M, Kueth C, et al. (2023). PIKFYVE inhibition mitigates disease in models of diverse forms of ALS. Cell 186, 786–802.e28. 10.1016/j.cell.2023.01.005. [PubMed: 36754049]

22. Shi Y, Kirwan P, Smith J, Robinson HPC, and Livesey FJ (2012). Human cerebral cortex development from pluripotent stem cells to functional excitatory synapses. Nat. Neurosci. 15, 477–486. 10.1038/nn.3041. [PubMed: 22306606]

23. Kim D-S, Lee DR, Kim H-S, Yoo J-E, Jung SJ, Lim BY, Jang J, Kang H-C, You S, Hwang D-Y, et al. (2012). Highly pure and expandable PSA-NCAM-positive neural precursors from human ESC and iPSC-derived neural rosettes. PLoS One 7, e39715. 10.1371/journal.pone.0039715.

24. Kwon I, Xiang S, Kato M, Wu L, Theodoropoulos P, Wang T, Kim J, Yun J, Xie Y, and McKnight SL (2014). Poly-dipeptides encoded by the C9orf72 repeats bind nucleoli, impede RNA biogenesis, and kill cells. Science 345, 1139–1145. 10.1126/science.1254917. [PubMed: 25081482]

25. Bennion Callister J, Ryan S, Sim J, Rollinson S, and Pickering-Brown SM (2016). Modelling C9orf72 dipeptide repeat proteins of a physiologically relevant size. Hum. Mol. Genet. 25, 5069–5082. 10.1093/hmg/ddw327. [PubMed: 27798094]

26. Cooper-Knock J, Higginbottom A, Stopford MJ, Highley JR, Ince PG, Wharton SB, Pickering-Brown S, Kirby J, Hautbergue GM, and Shaw PJ (2015). Antisense RNA foci in the motor neurons of C9ORF72-ALS patients are associated with TDP-43 proteinopathy. Acta Neuropathol. 130, 63–75. 10.1007/s00401-015-1429-9. [PubMed: 25943887]

27. Davidson Y, Robinson AC, Liu X, Wu D, Troakes C, Rollinson S, Masuda-Suzukake M, Suzuki G, Nonaka T, Shi J, et al. (2016). Neurodegeneration in frontotemporal lobar degeneration and motor neurone disease associated with expansions in C9orf72 is linked to TDP-43 pathology and not associated with aggregated forms of dipeptide repeat proteins. Neuropathol. Appl. Neurobiol. 42, 242–254. 10.1111/nan.12292. [PubMed: 26538301]

28. Zhang K, Daigle JG, Cunningham KM, Coyne AN, Ruan K, Grima JC, Bowen KE, Wadhwa H, Yang P, Rigo F, et al. (2018). Stress Granule Assembly Disrupts Nucleocytoplasmic Transport. Cell 173, 958–971.e17. 10.1016/j.cell.2018.03.025. [PubMed: 29628143]

29. Beatty KE, Liu JC, Xie F, Dieterich DC, Schuman EM, Wang Q, and Tirrell DA (2006). Fluorescence Visualization of Newly Synthesized Proteins in Mammalian Cells. Angew. Chem. 118, 7524–7527. 10.1002/ange.200602114.

30. Loveland AB, Svidritskiy E, Susorov D, Lee S, Park A, Zvornicanin S, Demo G, Gao F-B, and Korostelev AA (2022). Ribosome inhibition by C9ORF72-ALS/FTD-associated poly-PR and poly-GR proteins revealed by cryo-EM. Nat. Commun. 13, 2776. 10.1038/s41467-022-30418-0. [PubMed: 35589706]

31. Cao J, Spielmann M, Qiu X, Huang X, Ibrahim DM, Hill AJ, Zhang F, Mundlos S, Christiansen L, Steemers FJ, et al. (2019). The single-cell transcriptional landscape of mammalian organogenesis. Nature 566, 496–502. 10.1038/s41586-019-0969-x. [PubMed: 30787437]

32. Saunders A, Macosko EZ, Wysoker A, Goldman M, Krienen FM, de Rivera H, Bien E, Baum M, Bortolin L, Wang S, et al. (2018). Molecular Diversity and Specializations among the Cells of the Adult Mouse Brain. Cell 174, 1015–1030.e16. 10.1016/j.cell.2018.07.028. [PubMed: 30096299]

33. Liu Y, Pattamatta A, Zu T, Reid T, Bardhi O, Borchelt DR, Yachnis AT, and Ranum LPW (2016). C9orf72 BAC Mouse Model with Motor Deficits and Neurodegenerative Features of ALS/FTD. Neuron 90, 521–534. 10.1016/j.neuron.2016.04.005. [PubMed: 27112499]

34. Nguyen L, Laboissonniere LA, Guo S, Pilotto F, Scheidegger O, Oestmann A, Hammond JW, Li H, Hyysalo A, Peltola R, et al. (2020). Survival and Motor Phenotypes in FVB C9–500 ALS/FTD BAC Transgenic Mice Reproduced by Multiple Labs. Neuron 108, 784–796.e3. 10.1016/j.neuron.2020.09.009. [PubMed: 33022226]

35. Mordes DA, Morrison BM, Ament XH, Cantrell C, Mok J, Eggan P, Xue C, Wang J-Y, Eggan K, and Rothstein JD (2020). Absence of Survival and Motor Deficits in 500 Repeat C9ORF72 BAC Mice. Neuron 108, 775–783.e4. 10.1016/j.neuron.2020.08.009. [PubMed: 33022228]

36. Hagey DW, Topcic D, Kee N, Reynaud F, Bergsland M, Perlmann T, and Muhr J. (2020). CYCLIN-B1/2 and -D1 act in opposition to coordinate cortical progenitor self-renewal and lineage commitment. Nat. Commun. 11, 2898. 10.1038/s41467-020-16597-8. [PubMed: 32518258]

37. Wang L, Bluske KK, Dickel LK, and Nakagawa Y. (2011). Basal progenitor cells in the embryonic mouse thalamus - their molecular characterization and the role of neurogenins and Pax6. Neural Dev. 6, 35. 10.1186/1749-8104-6-35. [PubMed: 22077982]

38. Gressens P, Hill JM, Gozes I, Fridkin M, and Brenneman DE (1993). Growth factor function of vasoactive intestinal peptide in whole cultured mouse embryos. Nature 362, 155–158. 10.1038/362155a0. [PubMed: 8383805]

39. Hill JM, Hauser JM, Sheppard LM, Abebe D, Spivak-Pohis I, Kushnir M, Deitch I, and Gozes I. (2007). Blockage of VIP during mouse embryogenesis modifies adult behavior and results in permanent changes in brain chemistry. J. Mol. Neurosci. 31, 183–200. 10.1385/jmn:31:03:185. [PubMed: 17726225]

40. Passemard S, El Ghouzzi V, Nasser H, Verney C, Vodjdani G, Lacaud A, Lebon S, Laburthe M, Robberecht P, Nardelli J, et al. (2011). VIP blockade leads to microcephaly in mice via disruption of Mcph1-Chk1 signaling. J. Clin. Invest. 121, 3071–3087. 10.1172/JCI43824. [PubMed: 21737879]

41. Murphy NA, Arthur KC, Tienari PJ, Houlden H, Chiò A, and Traynor BJ (2017). Age-related penetrance of the C9orf72 repeat expansion. Sci. Rep. 7, 2116. 10.1038/s41598-017-02364-1. [PubMed: 28522837]

42. Akimoto C, Volk AE, van Blitterswijk M, Van den Broeck M, Leblond CS, Lumbroso S, Camu W, Neitzel B, Onodera O, van Rheenen W, et al. (2014). A blinded international study on the reliability of genetic testing for GGGGCC-repeat expansions in C9orf72 reveals marked differences in results among 14 laboratories. J. Med. Genet. 51, 419–424. 10.1136/jmedgenet-2014-102360. [PubMed: 24706941]

43. Zu T, Liu Y, Bañez-Coronel M, Reid T, Pletnikova O, Lewis J, Miller TM, Harms MB, Falchook AE, Subramony SH, et al. (2013). RAN proteins and RNA foci from antisense transcripts in C9ORF72 ALS and frontotemporal dementia. Proc. Natl. Acad. Sci. USA 110, E4968–E4977. 10.1073/pnas.1315438110. [PubMed: 24248382]

Highlights

- The *C9ORF72* repeat expansion alters neurogenesis

- LRRC47 plays a role in neural stem cell maintenance and is affected by poly(AP)

- Embryonic *C9ORF72* mice display decreases in thalamic volume and cortical thickness

- Neurodevelopmental perturbations induce early-onset motor deficits in *C9ORF72* mice
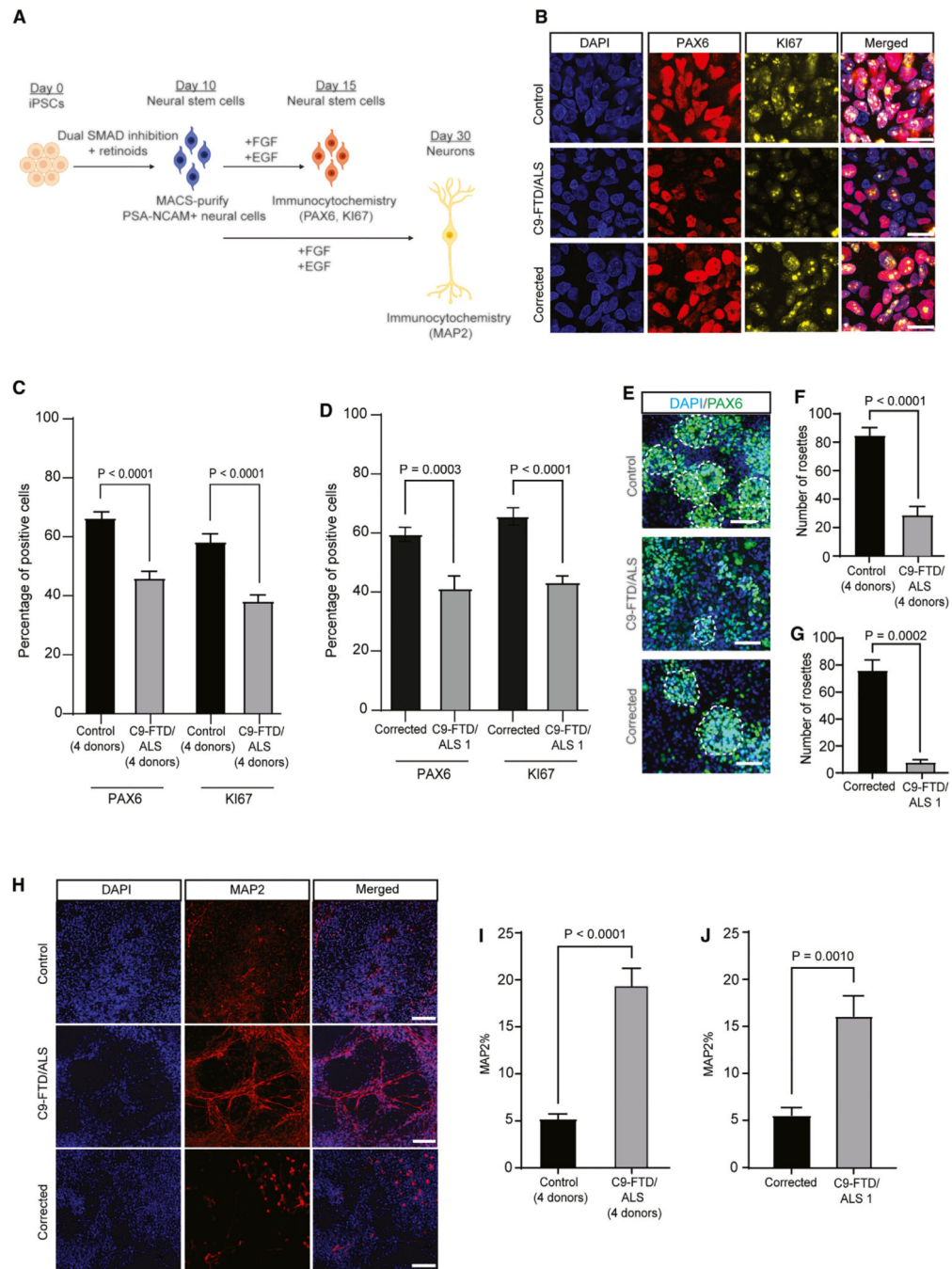
Figure 1. *C9ORF72* FTD/ALS neural stem cells exhibit poor self-renewal and precocious differentiation

(A) Schematic of neural stem and progenitor cell induction and timing of immunocytochemistry analysis for PAX6, KI67, and MAP2.

(B) Representative immunocytochemistry images of the percentages of PAX6+ and KI67+ neural stem and progenitor cells in control, *C9ORF72* FTD/ALS, and isogenic control (corrected) lines after MACS purification of PSA-NCAM+ cells on day 10 of neural differentiation and 5 additional days of culture with EGF and FGF. Scale bars, 25 μm.

(C) Quantification of the percentages of PAX6+ and KI67+ neural stem and progenitor cells in control and *C9ORF72* FTD/ALS lines after 5 additional days of culture with EGF and FGF after MACS purification of PSA-NCAM+ cells.

(D) Quantification of the percentages of PAX6+ and KI67+ neural stem and progenitor cells in the corrected or *C9ORF72* FTD/ALS line 1 after 5 additional days of culture with EGF and FGF after MACS purification of PSA-NCAM+ cells.

(C and D) Data are shown as mean ± SEM and were analyzed using a 2-way ANOVA with Sidak's correction.

(E) Representative immunocytochemistry images of rosette-like structures of PAX6+ cells in control, *C9ORF72* FTD/ALS, and corrected lines after MACS purification of PSA-NCAM+ cells on day 10 of neural differentiation and 5 additional days of culture with EGF and FGF. Scale bars, 100 μm. Examples of manually counted rosettes are outlined.

(F) Quantification of the total number of PAX6+ rosette-like structures formed in control or *C9ORF72* FTD/ALS cultures.

Quantification of the total number of PAX6+ rosette-like structures formed in corrected or *C9ORF72* FTD/ALS line 1 cultures.

(F and G) Data are shown as mean ± SEM and were analyzed using an unpaired t test. Each independent differentiation was used as a data point.

(H) Representative immunocytochemistry images of the number of MAP2+ neurons in control, *C9ORF72* FTD/ALS, and corrected line cultures after MACS purification of PSA-NCAM+ cells on day 10 of neural differentiation and 20 additional days of culture with EGF and FGF. Scale bars, 100 μm.

(I) Quantification of the total number of MAP2+ neurons formed in control or *C9ORF72* FTD/ALS cultures on day 30 with EGF and FGF.

(J) Quantification of the total number of MAP2+ neurons formed in corrected or *C9ORF72* FTD/ALS cultures at day 30 with EGF and FGF.

(I and J) Data are shown as mean ± SEM and were analyzed using an unpaired t test.

(A–J) The data points for each group include 3 independent differentiations with 2 technical replicates from each line. Each independent differentiation was used as a data point.
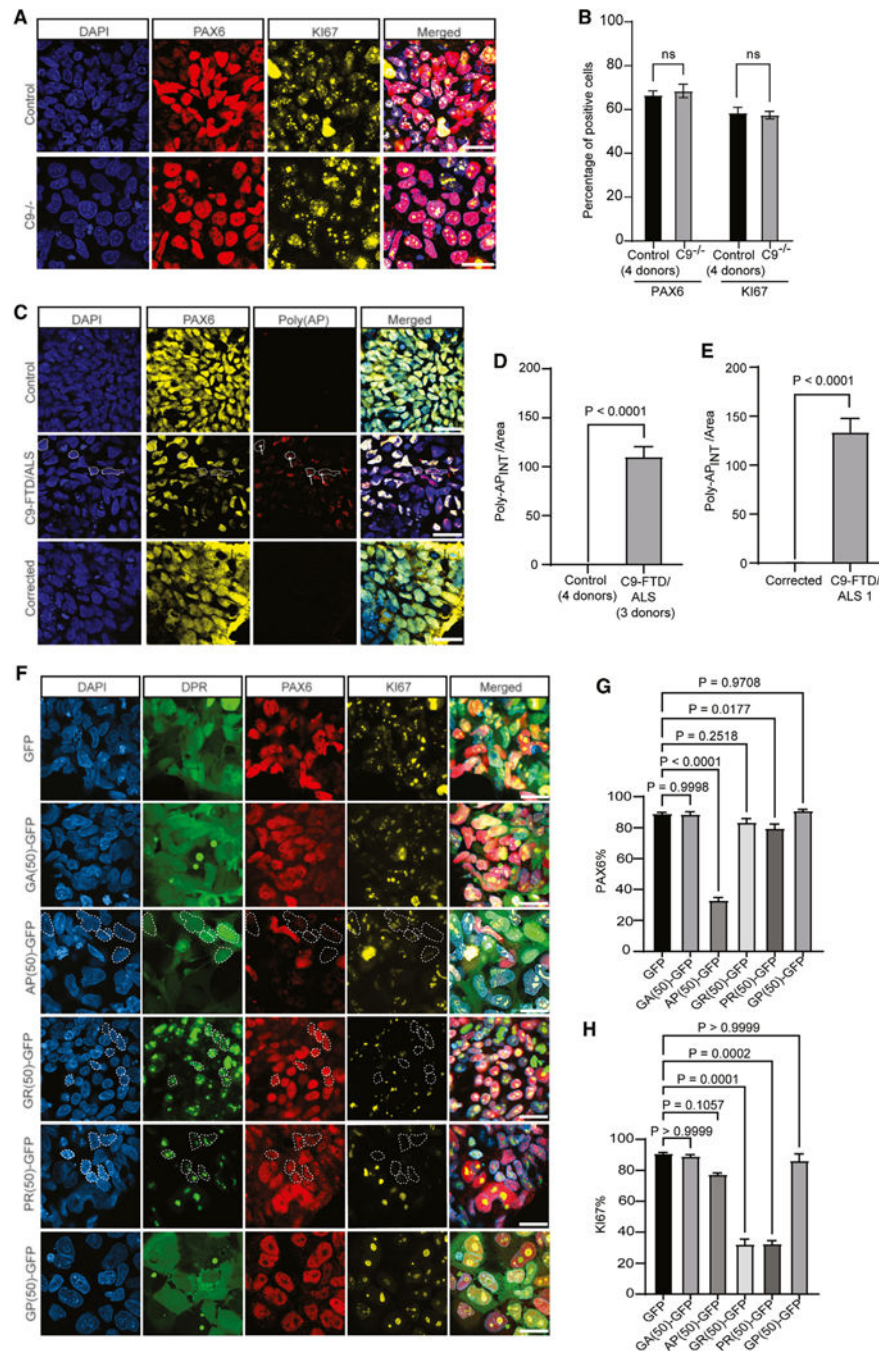
Figure 2. Poly(AP) and other C9ORF72 DPRs impair neural stem cell self-renewal

(A) Representative images of the percentages of PAX6+ cells in control and *C9ORF72*$^{-/-}$ cultures after MACS purification of PSA-NCAM+ cells on day 10 of neural differentiation and 5 additional days of culture with EGF and FGF. Scale bars, 25 μm.

(B) Quantification of the percentages of PAX6+ and KI67+ neural stem and progenitor cells in control and *C9ORF72*$^{-/-}$ cultures on day 15 with EGF and FGF. Data are shown as the mean ± SEM and were analyzed using an unpaired t test. n.s., not significant.

(C) Representative immunocytochemistry images of poly(AP) levels in control, *C9ORF72* FTD/ALS, or corrected cultures on day 10 of neural differentiation. Scale bars, 30 μm.

(D) Quantification of poly(AP) intensity normalized to cell area in PAX6+ cells from control or *C9ORF72* FTD/ALS cultures on day 10 of neural differentiation.

(E) Quantification of poly(AP) intensity normalized to cell area in PAX6+ cells from corrected or *C9ORF72* FTD/ALS line 1 cultures on day 10 of neural differentiation.

(D and E) Data are shown as mean ± SEM and were analyzed with an unpaired t test (D) or a Mann-Whitney unpaired t test (E).

(F) Representative immunocytochemistry images of the percentages of PAX6+ and Ki67+ cells in control line cultures after MACS purification of PSA-NCAM+ cells on day 10 of neural differentiation; transduction with GFP, GA(50)-GFP, AP(50)-GFP, GR(50)-GFP, PR(50)-GFP, or (GP)50-GFP; and 5 additional days of culture with EGF and FGF. Outlines depict cells that are PAX6 negative or KI67 negative in cells transduced with AP(50)-GFP and PR/GR(50)-GFP, respectively. Scale bars, 25 μm.

(G and H) Quantification of immunocytochemical analysis of the percentages of PAX6+ (G) and Ki67+ (H) cells in control line cultures after MACS purification of PSA-NCAM+ cells and transduction with GFP or DPR-GFP lentiviruses on day 10 of neural differentiation and 5 additional days of culture with EGF and FGF. Values are represented as the mean ± SEM and were analyzed using a one-way ANOVA (G) or Kruskal-Wallis test (H).

(A–H) The data points for each group include 3 independent differentiations with 2 technical replicates per line per condition. Each independent differentiation was used as a data point.
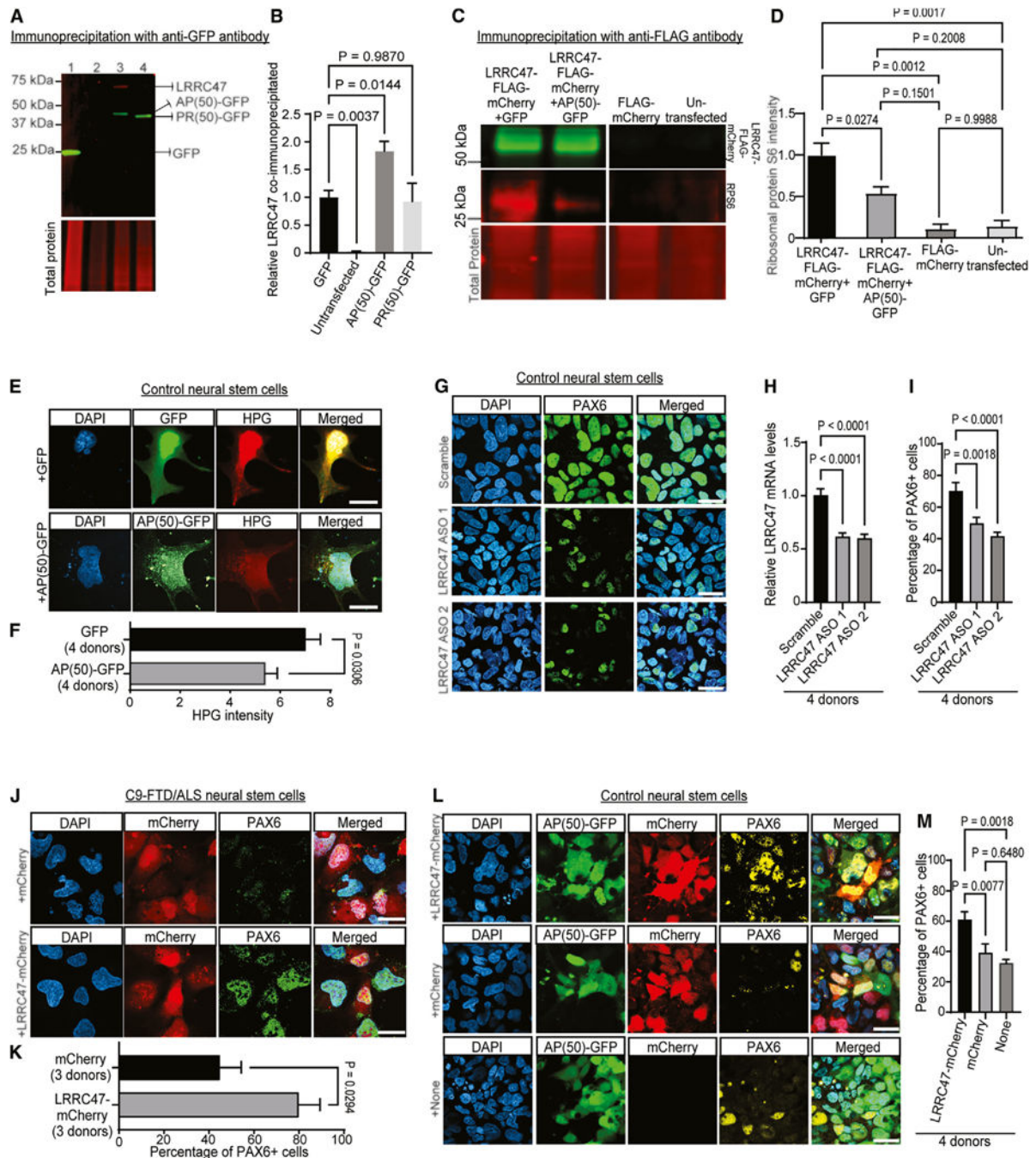
Figure 3. Poly(AP) impairs neural stem cell maintenance through LRRC47

(A) Representative western blot image of endogenous LRRC47 co-immunoprecipitated with GFP, untransfected control, AP(50)-GFP, or PR(50)-GFP from HEK293T cells using an anti-GFP antibody.

(B) Quantification of western blot analysis of LRRC47 levels co-immunoprecipitated with GFP, untransfected control, AP(50)-GFP, or PR(50)-GFP using an anti-GFP antibody. Data are shown as the amount of LRRC47 co-immunoprecipitated normalized to the amount of GFP immunoprecipitated for each sample. Data points for each group consist of 3

independent transfections with 3 technical replicates for each transfection. LRRC47 levels were normalized to total protein for each sample. Mean ± SEM. Unpaired t test.

(C) Representative western blot image of endogenous RPS6 co-immunoprecipitated with a LRRC47-FLAG-mCherry fusion protein in HEK293T cells overexpressing GFP or AP(50)-GFP. Co-immunoprecipitation with FLAG-mCherry was used as a control for any potential interaction between RPS6 and FLAG-mCherry.

(D) Quantification of western blot analysis of the RPS6 levels co-immunoprecipitated with either LRRC47-FLAG-mCherry or FLAG-mCherry in HEK293T cells overexpressing GFP or AP(50)-GFP. Data points for each group consist of 3 independent transfections. Each independent differentiation was used as a data point. RPS6 levels were normalized to total protein for each sample. Mean ± SEM. One-way ANOVA with Tukey's correction.

(E) Representative images of homopropargylglycine (HPG)-Alexa Fluor 594 incorporation into control MACS-purified PSA-NCAM+ cells after transduction with GFP or AP(50)-GFP lentiviruses and further culture for 5 days with EGF and FGF. Scale bar, 10 μm.

(F) Quantification of HPG incorporation into newly synthesized proteins in control MACS-purified PSA-NCAM+ cells. Data points consist of 2 independent differentiations from 4 different control lines with 2 technical replicates per line per condition. Each independent differentiation was used as a data point. Mean ± SEM. Unpaired t test.

(G–I) Representative immunocytochemistry images (G), relative *LRRC47* mRNA levels after ASO treatment (H), and quantification (I) of the percentage of PAX6+ cells in control line cultures after MACS purification of PSA-NCAM+ cells and treatment with scrambled or *LRRC47*-suppressing ASOs on day 10 of neural differentiation and 5 additional days of culture with EGF and FGF. Mean ± SEM. The data points for each group include 2 independent differentiations per line per condition (4 control lines). Each independent differentiation was used as a data point. One-way ANOVA with Dunnett's correction. Scale bars, 25 μm.

(J and K) Representative immunocytochemistry images (J) and quantification (K) of the percentage of PAX6+ cells in control or *C9ORF72* FTD/ALS cultures after MACS purification of PSA-NCAM+ cells and transduction with mCherry- or LRRC47-mCherry-encoding lentiviruses on day 10 of neural differentiation and 5 additional days of culture with EGF and FGF. Mean ± SEM. The data points for each group include 2 independent differentiations with 2 technical replicates per line per condition. Each independent differentiation was used as a data point. Unpaired t test. Scale bars, 15 μm.

(L and M) Representative immunocytochemistry images (L) and quantification (M) of the percentage of PAX6+ cells in control line cultures after MACS purification of PSA-NCAM+ cells and transduction with lentiviruses encoding AP(50)-GFP and either LRRC47-mCherry, mCherry alone, or no additional lentivirus on day 10 of neural differentiation and 5 additional days of culture with EGF and FGF. The data points for each group include 2 independent differentiations per line per condition. Each independent differentiation was used as a data point. Mean ± SEM. One-way ANOVA with Tukey's correction. Scale bars, 25 μm.
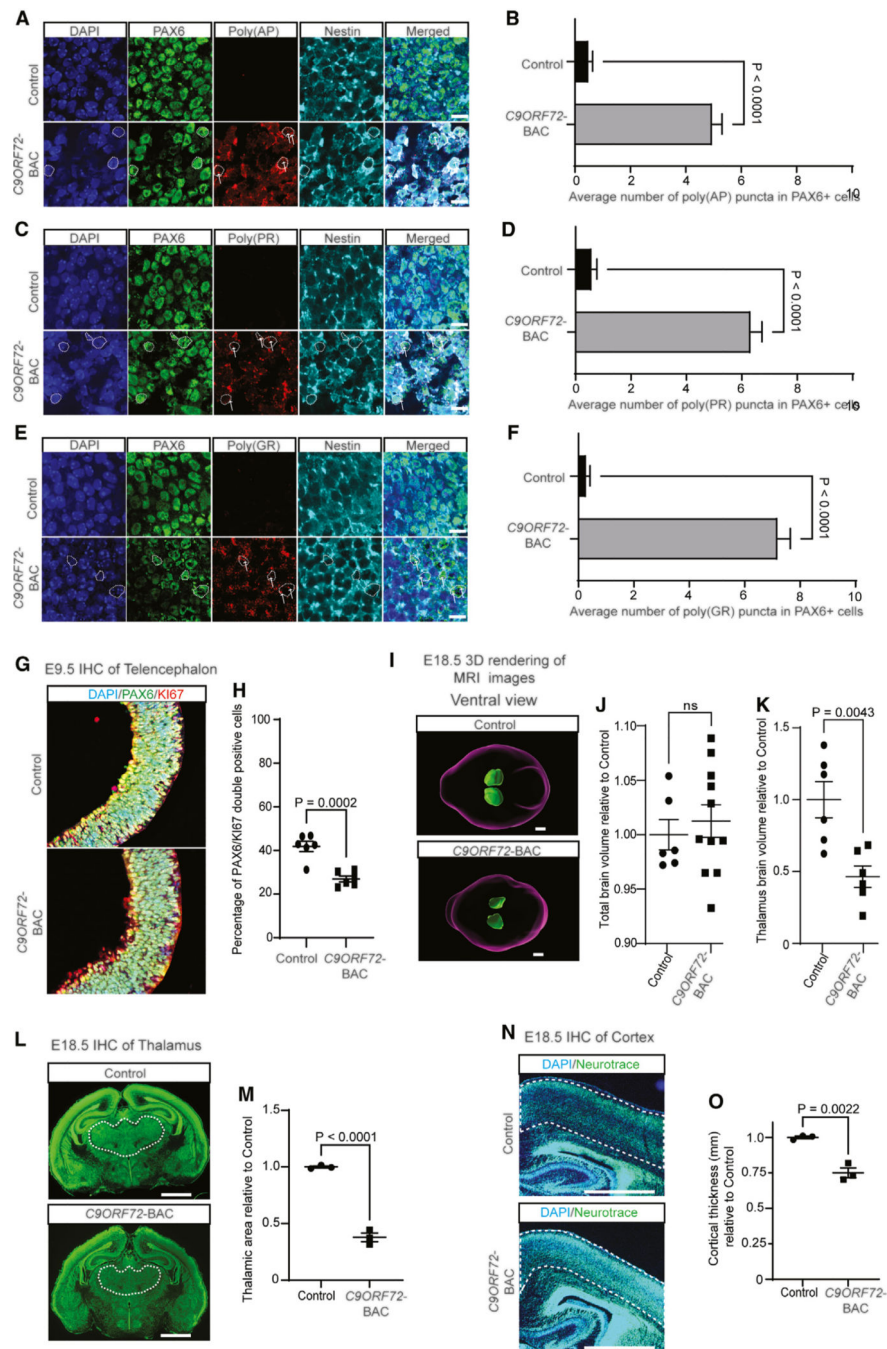
Figure 4. The C9ORF72 repeat expansion reduces thalamic and cortical size in embryonic mice (A and B) Representative immunocytochemistry images

(A) and quantification (B) of the number of poly(AP)+ puncta in PAX6+ cortical progenitor cells in E9.5 control or *C9ORF72*-BAC embryos.

(C and D) Representative immunocytochemistry images (C) and quantification (D) of the number of poly(PR)+ puncta in PAX6+ cortical progenitor cells in E9.5 control or *C9ORF72*-BAC embryos.

(E and F) Representative immunocytochemistry images (E) and quantification (F) of the number of poly(GR)+ puncta in PAX6+ cortical progenitor cells in E9.5 control or *C9ORF72*-BAC embryos.

(A–F) Outlines depict PAX6+ cells, and the arrows point toward DPR puncta. NESTIN was used to identify cell boundaries to determine whether endogenous DPRs were localized intra/extracellularly. Data points consist of the average number of DPR puncta per progenitor cell in 3 control and 3 *C9ORF72*-BAC embryos for each DPR. Each data point represents one embryo. Approximately 20 progenitor cells were quantified per embryo. Data are shown as mean ± SEM and were analyzed using an unpaired t test (B and F) or a Mann-Whitney t test (D). Scale bars, 10 μm.

(G and H) Representative images (G) and quantification of PAX6 and KI67 double-positive cells (H) in the developing telencephalon of E9.5 control (n = 6) or *C9ORF72*-BAC (n = 6) embryos. Each data point represents one embryo. Mean ± SEM. Unpaired t test.

(I) Representative 3D renderings of magnetic resonance imaging of E18.5 control and *C9ORF72*-BAC embryos showing total brain and thalamic volume. The brains are oriented from a ventral perspective with the olfactory bulbs on the left. Purple outlines the brain, and the thalamic regions are colored green. Scale bars, 1 mm.

(J) Quantification of total brain volume normalized to body weight for E18.5 control and *C9ORF72*-BAC embryos. Magnetic resonance imaging was used for quantification. Each data point represents the relative ratio of total brain volume normalized to body weight for one embryo (n = 6 control and 11 *C9ORF72*-BAC embryos). Mean ± SEM. Unpaired t test.

(K) Quantification of thalamic volume normalized to total brain volume for E18.5 control and *C9ORF72*-BAC embryos. Magnetic resonance imaging was used for quantification. Each data point represents the relative ratio of thalamic brain volume to total brain volume for one embryo (n = 6 control and 6 *C9ORF72*-BAC embryos). Mean ± SEM. Unpaired t test.

(L and M) Representative images (L) and quantification (M) of relative thalamic area in E18.5 control and *C9ORF72*-BAC embryos using immunohistochemistry. Data points represent the relative ratio of thalamic area in 3 control and 3 *C9ORF72*-BAC embryos. Each data point represents one embryo. The average area of the thalamus was determined starting at approximately bregma + 3.51 μm, followed by an additional 3 sections at 16 μm each. Mean ± SEM. Unpaired t test.

Scale bars, 1 mm.

(N and O) Representative images (N) and quantification (O) of relative cortical thickness in E18.5 control and *C9ORF72*-BAC embryos using immunohistochemistry. Data points represent the relative ratio of cortical thickness in one embryo for 3 control and 3 *C9ORF72*-BAC embryos. The average cortical thickness was determined by measuring the width from layer 1 to layer 6 across 3 different 16-μm sections. Mean ± SEM. Unpaired t test. Scale bars, 1 mm.
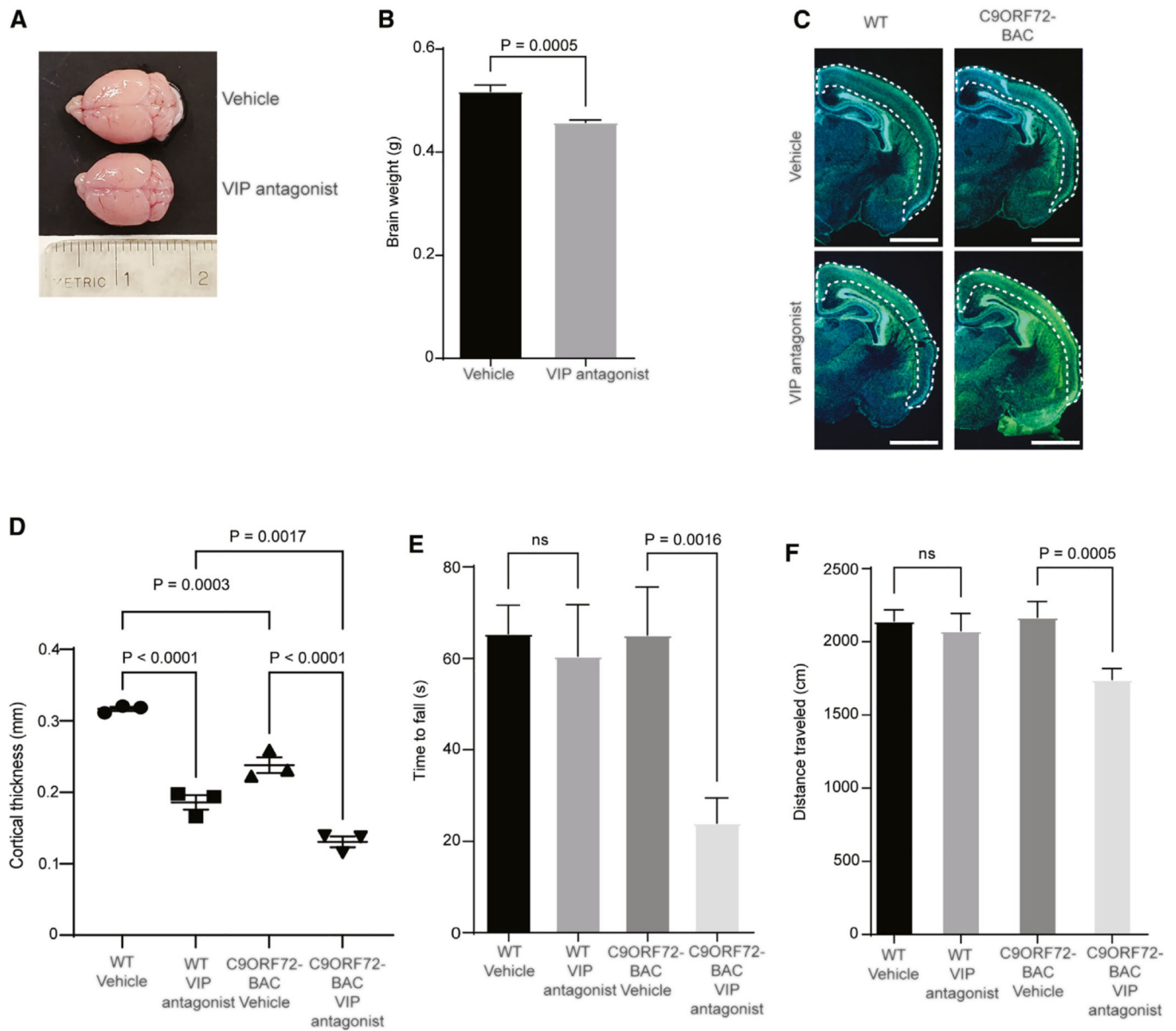
Figure 5. Reducing brain volume triggers symptom onset in *C9ORF72*-BAC mice

(A) Representative images of brains of 2-month-old mice exposed to vehicle or 2 μg/g VIP antagonist from E9.5–E11.5.

(B) Quantification of brain mass in 2-month-old mice that were treated with vehicle or VIP antagonist from E9.5–E11.5. Each data point represents the brain mass of one mouse (n = 9 vehicle and n = 8 VIP antagonist). Mean ± SEM. Unpaired t test.

(C and D) Representative images (C) and quantification (D) of cortical thickness in E18.5 control and *C9ORF72*-BAC embryos treated with vehicle or 2 μg/g VIP antagonist using immunohistochemistry. Each data point represents the average cortical thickness in one embryo (n = 3 control and 3 *C9ORF72*-BAC embryos). The average cortical thickness was determined by measuring the width from layer 1 to layer 6 across 3 different 16-mm sections

beginning at approximately bregma + 3.51. Mean ± SEM. One-way ANOVA. Scale bars, 1 mm.

(E) Quantification of time to fall in a hanging wire test for 2-month-old control and *C9ORF72*-BAC mice treated with vehicle or VIP antagonist from E9.5–E11.5. Each data point represents the average time to fall for one mouse. Control + vehicle, n = 11 mice; control + VIP antagonist, n = 10 mice; *C9ORF72*-BAC + vehicle, n = 10 mice; *C9ORF72*-BAC + VIP antagonist, n = 16 mice. Mean ± SEM. Kruskal-Wallis test.

(F) Quantification of total distance traveled during an open field test for 2-month-old control and *C9ORF72*-BAC mice treated with vehicle or VIP antagonist from E9.5–E11.5. Each data point represents the total distance traveled for one mouse. Control + vehicle, n = 11 mice; control + VIP antagonist, n = 10 mice; *C9ORF72*-BAC + vehicle, n = 10 mice; *C9ORF72*-BAC + VIP antagonist, n = 16 mice. Mean ± SEM. two-way ANOVA.

KEY RESOURCES TABLE

REAGENT or RESOURCE	SOURCE	IDENTIFIER
Antibodies		
PAX6 (Mouse IgG1)	Thermo Fisher	Cat# MA1-109; RRID: AB_2536820
PAX6 (Rabbit IgG)	Biolegend	Cat# 901301; RRID: AB_2565003
PAX6 (Mouse IgG1)	Santa Cruz Biotechnology	Cat# sc-81649; RRID: AB_1127044
NESTIN (Chicken IgY)	Novus Biologicals	Cat# NB100-1604; RRID: AB_2282642
KI67 (Rabbit IgG)	GeneTex	Cat# GTX16667; RRID: AB_422351
KI67 (Mouse IgG1)	BD Biosciences	Cat# 550609; RRID: AB_393778
MAP2 (Chicken IgY)	Abcam	Cat# ab5392; RRID: AB_2138153
Caspase 3 (Rabbit IgG)	Abcam	Cat# ab13847; RRID: AB_443014
Poly(AP) repeat (Rabbit IgG)	Proteintech	Cat# 24493-1-AP; RRID: AB_2879572
Poly(PR) repeat (Rabbit IgG)	Proteintech	Cat# 23979-1-AP; RRID: AB_2879388
Poly(GR) repeat (Rabbit IgG)	Proteintech	Ca# 23978-1-AP; RRID: AB_2879387
GFP (Chicken IgY)	Aves	Cat# GFP-1010; RRID: AB_2307313
LRRC47 (Rabbit IgG)	Proteintech	Cat# 23217-1-AP; RRID: AB_2879234
RPS6 (Mouse IgG1)	Thermo Fisher	Cat# MA5-15123; RRID: AB_10999800
C9ORF72 (Rabbit IgG)	Proteintech	Cat# 22637-1-AP; RRID: AB_10953528
PSA-NCAM magnetic microbeads	Miltenyi	Cat# 130-092-966
FLAG M2 magnetic beads	Sigma	Cat# M8823; RRID: AB_2637089
Donkey anti-Mouse, IgG (H + L) Highly Cross-Adsorbed, Alexa Fluor® 488	Invitrogen	Cat# A-21202; RRID: AB_141607
Donkey anti-Mouse, IgG (H + L) Highly Cross-Adsorbed, Alexa Fluor® 555	Invitrogen	Cat# A-31570; RRID: AB_2536180
Donkey anti-Rabbit, IgG (H + L) Highly Cross-Adsorbed, Alexa Fluor® 488	Invitrogen	Cat# A-21206; RRID: AB_2535792
Donkey Anti-Chicken IgY (IgG) (H + L) Alexa Fluor® 647	Jackson ImmunoResearch	Cat# 703-605-155; RRID: AB_2340379
IRDye® 680RD Donkey anti-Rabbit IgG Secondary Antibody	LI-COR Biosciences	Cat# 926-68073; RRID: AB_10954442
IRDye® 800CW Donkey anti-Mouse IgG Secondary Antibody	LI-COR Biosciences	Cat# 926-32212; RRID: AB_621847
Bacterial and virus strains		
mCherry (Lentivirus)	Genecopoeia	EX-NEG-Lv216
LRRC47-mCherry (Lentivirus)	Genecopoeia	EX-T4416-Lv216
GFP (Lentivirus)	Wen etal. 2014[10]	N/A
GA(50)-GFP (Lentivirus)	Wen etal. 2014[10]	N/A
GP(50)-GFP (Lentivirus)	Wen etal. 2014[10]	N/A
GR(50)-GFP (Lentivirus)	Wen etal. 2014[10]	N/A
PR(50)-GFP (Lentivirus)	Wen etal. 2014[10]	N/A
AP(50)-GFP (Lentivirus)	Wen etal. 2014[10]	N/A
Chemicals, peptides, and recombinant proteins		

REAGENT or RESOURCE	SOURCE	IDENTIFIER
Y-27632 2HCl	Selleckchem	S1049
Knockout serum replacement	Thermo Fisher	10828028
SB 431542	Cayman Chemical	13031
LDN-193189	Cayman Chemical	11802
mTeSR1	StemCell Technologies	85851
N2	Gibco	17502048
B27	Gibco	17504044
Accutase	Innovative Cell Technologies	AT4104
Lenti-X concentrator	TaKaRa	631232
Penicillin-streptomycin 50X	Corning	30-001-Cl
Recombinant Human EGF	R&D Systems	236-EG-200
Recombinant Human FGF	R&D Systems	3718-FB-025
Glutamax	Gibco	35050-061
Non-Essential Amino Acids (100x)	Thermo Fisher	11140050
DMEM	Gibco	11995-065
Geltrex	Thermo Fisher	A1413201
FBS	GenClone	25-514
DAPI	Thermo Fisher	D1306
Propidium Iodide	Thermo Fisher	P3566
Vasoactive intestinal peptide receptor antagonist	Tocris	3054
Prohance	Bracco Diagnostics Inc.	NDC 0270-1111-70
Protease inhibitor cocktail	Sigma	4693132001
Pierce IP lysis buffer	Thermo Fisher	87787
3x FLAG peptide	Sigma	F4799
Critical commercial assays		
GFP-trap magnetic particles M-270 kit	Chromotek	Gtdk-20
Click-iT™ HPG Alexa Fluor™ 594 protein synthesis assay kit	Thermo Fisher	C10429
DNeasy blood and tissue kit	Qiagen	69504
RNeasy plus mini kit	Qiagen	74136
ProtoScript II first strand synthesis kit	NEB	102855-124
Deposited data		
Bulk RNA-seq data derived from day 10 neural stem cells	This manuscript	GSE238005
Experimental models: Cell lines		
ND03231 (Control 1)	NINDS Biorepository	3231
ND03719 (Control 2)	NINDS Biorepository	3719
ND00184 (Control 3)	NINDS Biorepository	00184
ND05280 (Control 4)	NINDS Biorepository	5280

REAGENT or RESOURCE	SOURCE	IDENTIFIER
ND06769 (C9-FTD/ALS 1)	NINDS Biorepository	6769
ND12099 (C9-FTD/ALS 2)	NINDS Biorepository	12099
ND10689 (C9-FTD/ALS 3)	NINDS Biorepository	10689
ND12100 (C9-ALS 4)	NINDS Biorepository	12100
Isogenic corrected (parental line = ND06769)	This paper	N/A
C9ORF72 homozygous knockout (parental line = ND03231)	This paper	N/A
Experimental models: Organisms/strains		
Wild-type FVB/NJ	The Jackson Laboratory	001800
FVB/NJ-Tg(C9orf72)500Lpwr/J	The Jackson Laboratory	029099
Oligonucleotides		
*LRRC47*ASO 1	This paper	/52MOErA/*/i2MOErC/*/i2MOErT/* /i2MOErG/*/ i2MOErG/*T* G*G*C*A*C*T* T*G*T* / i2MOErT/*/i2MOErA/*/i2MOErC/*/i2MOErT/*/ 32MOErT/
LRRC47ASO 2	This paper	/52MOErC/*/i2MOErT/*/i2MOErT/*/i2MOErT/* / i2MOErC/*C* A*G*C*A*C*T* G*G*G*/i2MOErA/* / i2MOErT/*/i2MOErT/*/i2MOErC/*/32MOErG/
C9ORF72 antisense transcript suppressing ASO	This paper	/52MOErG//i2MOErG//i2MOErT//i2MOErG// i2MOErG/C*G*A*G*T*G*G*T*G/i2MOErA// i2MOErG//i2MOErT//i2MOErG//32MOErA/
CRISPRs sgRNA-1 targeting upstream of repeat expansion	This paper	GUAACCUACGGUGUCCCGCU
CRISPR sgRNA-2b targeting downstream of repeat expansion (– strand)	This paper	ACCCCAAACAGCCACCCGCC
Scramble ASO	This paper	/52MOErG/*/i2MOErC/*/i2MOErG/*/i2MOErA/* / i2MOErC/*T* A*T*A*C*G*C* G*C*A*/i2MOErA/* / i2MOErT/*/i2MOErA/*/i2MOErT/*/32MOErG/
RP-PCR primer 1	Akimoto et al. 2014[42]	FAM-TGTAAAACGACGGCCAGTCAAGGAG GGAAACAACCGCAGCC
RP-PCR primer 2	Akimoto et al. 2014[42]	CAGGAAACAGCTATGACCGGGCCCGCCC CGACCACGCCCCGGCCCCGGCCCCGG
RP-PCR primer 3	Akimoto et al. 2014[42]	CAGGAAACAGCTATGACC
Forward primer for *C9ORF72* Southern blot probe	This paper	AGAACAGGACAAGTTGCC
Reverse primer for *C9ORF72* Southern blot probe	This paper	AACACACACCTCCTAAACC
LRRC47 RT-qPCR forward primer	This paper	GAGCAGAGGAAGCAGAAGAAG
LRRC47 RT-qPCR reverse primer	This paper	CATCCACAAGACACGGGTAAT
C9ORF72-BAC genotyping forward primer	The Jackson Laboratory	TCGAAATGCAGAGAGTGGTG
LK-AS-ORF-R	Zu etal. 2013[43]	CGACTGGAGCACGAGGACACTGACGAGTGG G TGAGTGAGGAG
AS-ORF-F	Zu etal. 2013[43]	CGACTGGAGCACGAGGACACTGAAGTCGCTA G AGGCGAAAGC
LK primer	Zu etal. 2013[43]	CGACTGGAGCACGAGGACACTGA
C9ORF72-BAC genotyping reverse primer	The Jackson Laboratory	CTTCCTTTCCGGATTATATGTG

REAGENT or RESOURCE	SOURCE	IDENTIFIER
Internal genotyping control forward primer	The Jackson Laboratory	CTGTCCCTGTATGCCTCTGG
Internal genotyping control reverse primer	The Jackson Laboratory	AGATGGAGAAAGGACTAGGCTACA
Software and algorithms		
ImageJ	*Publicly available*	https://imagej.nih.gov/ij/
Prism	Graphpad	https://www.graphpad.com/scientific-software/prism/
Enrichr	*Publicly available*	https://maayanlab.cloud/Enrichr/
Imaris	Imaris	https://imaris.oxinst.com/
Peak Scanner app	Thermo Fisher	https://apps.thermofisher.com/
Noldus Ethovision software	Noldus	https://www.noldus.com/